2011-01-01

Asphaltene As Light Harvesting Material In Dye Sensitized Solar Cell

Rajab Emhemed Abujnah
University of Texas at El Paso, reabujnah@miners.utep.edu

ASPHALTENE AS LIGHT HARVESTING MATERIAL IN DYE SENSITIZED SOLAR CELL

RAJAB EMHEMED ABUJNAH

Department of Environmental Science and Engineering

APPROVED:

Russell R. Chianelli , Ph.D., Chair

Roy Arrowood , Ph.D

Felicia Manciu, Ph.D.

Jose Nunez, Ph.D.

Benjamin Flores, Ph.D.
Acting Dean of the Graduate School

Dedication

I dedicate this work to my Mom Mabruka Ali Albakush in her graveyard ask God to forgive her and Dad Emhemed Khalifa Abujnah ask God to give him longer healthy life. They gave me birth, raised me, loved me and supported me. I devote this work to them for their love and support, their love of education, the huge sacrifices they made to guarantee I get to the highest level of education, and for everything they have done to me.

أهداء

اهدى هدا العمل الى والديا المرحومة امى مبروكة على البكوش اسئل الله العلى العظيم ان يرحمها و يغفرلها وابى العزبز امحمد خليفة ابوجناح اسئل الله ان يطيل فى عمره ويشفيه

اهدى لهم هدا العمل لما قدموه لى من تضحيات معنوية وروحية واقتصادية ولاصرارهم الحثيث على الحصول على اعلى الشهائد العلمية واقول لهم ان ابنكم البار لم ولن ينسي تضحياتكم ولولاكم ما اتيت الي هده الدنيا ولولا رعايتكم وتربيتكم وتعليمكم لما وصلت الى هده الدرجة العلمية

ASPHALTENE AS LIGHT HARVESTING MATERIAL IN DYE SENSITIZED SOLAR CELL

by

RAJAB EMHEMED ABUJNAH, M.Sc.

DISSERTATION

Presented to the Faculty of the Graduate School of

The University of Texas at El Paso

in Partial Fulfillment

of the Requirements

for the Degree of

DOCTOR OF PHILOSOPHY

Department of Environmental Science and Engineering

THE UNIVERSITY OF TEXAS AT EL PASO

August 2011

Acknowledgements

About four and half years ago I started this life time dream journey and today I proudly stand at the end of it, seeing the light and heading gradually towards it. It has been an important stage of my life full of various experiences, with all its ups and downs, has added a lot more to my professional and personal developments. There were times it felt like I was in a battle situation and the only option was to keep advancing, regardless of the magnitude of obstacles on the way. Withdrawing or giving up has never been an option as I cannot afford to fail. I have finished the race and I have kept the faith. Special thanks to the almighty God for His compassion, mercy and grace, and for being in control over every situation.

I would like to take this opportunity and express my sincere appreciation to those that have made my life time dream come true. First on the list is my Ph.D. advisor, Prof, Russell R. Chianelli for his significant guidance during my Ph.D. program study in the Department of Environmental Science and Engineering. He was the main actor in developing my research interest and directed me to a meaningful understanding of research methodology in science and technology. Not only did he teach me science, he taught me how to get the core out of vague ideas, and how to think about and approach problems and I will be able to use these training lessons all over my career. Chianelli has modeled the art of being an advisor. He continuously allow me discover the ideas I found interesting and was there with encouragement and good ideas when I needed them. He is also an amazing role model both professionally and personally and I hope to be able to follow his example. This dissertation would not have been possible without his careful supervision. His inspiration, enthusiasm, suggestions and encouragements have helped me to improve my research skills, expand my scientific imagination and defeat difficult scientific challenges.

I greatly thankful to all the members of my dissertation committee, Professor Roy Arrowood, Professor Felicia Manciu, and Professor Jose Nunez for listening to my "lectures" and for their feedback, and for devoting their time and expertise to review my dissertation. In addition, I would like to thank Dr. Michael Irwin for his help in the dye sensitized solar cell testing, the results of which I am presenting in this dissertation.

Special gratitude to my beloved wife Mabruka Hadidan and also to my siblings: Muhaned, Amany, Tahani and my little one Aya for their emotional support every step of the way and for their undying love. Special thanks also go to my brothers and sisters in Libya especially my older brother Hamed Abujnah and my older sister Fathia Abujnah for their continued and unparalleled support, generosity, love, and encouragement.

Nonetheless, my work and time in UTEP would have been far poorer without the academic and moral support from; Omar Al-Qudah, with whom I shared four years of friendship and study at UTEP; thank you for the time of discussion and encouragements and all the Libyan PhD's students at the Environmental Science and Engineering Department I wish you all the best on your PhD's and hope to meet you sometime in the future. I am very thankful to the Libyan Ministry of Higher Education, Canadian Bureau for International Education and Hunt Company for the financial support.

Lastly, and most importantly, I would like to express my heart full thank you to my parents; Emhemed Khalifa Abujnah and Mabruka Ali Albakush ask Allah to be kind to her. They gave my birth, raised me, taught me, encouraged me and loved me. They always believe their son is able to pursue a higher education in United States without any hesitation. To them I dedicate this dissertation.

Abstract

This dissertation characterizes the first asphaltene DSSC (dye-sensitized solar cell), in which light to electricity conversion efficiency has improved from 0 % to 1.8 %. Four natural organic asphaltene factions, namely, un-fractionated asphaltene, Fr. 1 Asphaltene, Fr.2 asphaltene, Fr.3 and Fr.4 were extracted and tested for various solar cell parameters of TiO_2 based dye-sensitized solar cell DSSC. DSSCs were fabricated using the four individual asphaltene dyes. The photovoltaic performance of the cells was examined by determining the various parameters such as open-circuit voltage, short-circuit current, fill factor, and series resistance. The overall energy conversion efficiency was also measured to correlate the effect of the different asphaltene fraction as well as concentration on the significant improvement of the solar cell parameters. The sensitization of TiO_2 electrode with fr.3 asphaltene obtained at 90/10 toluene to pentane ratio has resulted in a maximum energy conversion efficiency of 1.8 %. Un-fractionated asphaltene, however, produces comparable results as Fr.3 when used as sensitizer in DSSC. A strategy to minimize series resistance, and improve photo current as well as open circuit voltage is also studied. Purifying asphaltene, using RTV mask, and employing the TiO_2 compact layer as well as UV-O treatment have been shown to improve the performance of asphaltene DSSCs.

Table of Contents

List of Tables

List of Figures

List of Illustrations

Chapter: 1 Background and Motivation

1.1 INTRODUCTION

During the last few decades there have been major efforts to address the enormous growth of both the worldwide energy demand and the emissions of green house gases (GHG) that are due to burning of fossil fuels and other energy consumption. The Energy Information Administration (EIA) (1) of the U.S. Department of Energy reported that the global energy consumption increased by 22 % from 406 quadrillion Btu in 2000 to 495 Btu in 2007 and it is projected to grow by 49 percent or 1.4 percent per year, from 495 quadrillion Btu in 2007 to 739 quadrillion Btu in 2035 (figure 1.1). [1] Fossil fuels still provide nearly 80 percent of world energy consumption in 2010. Figure 1.1 shows the projected trend from the EIA's International Energy Outlook for 2010.

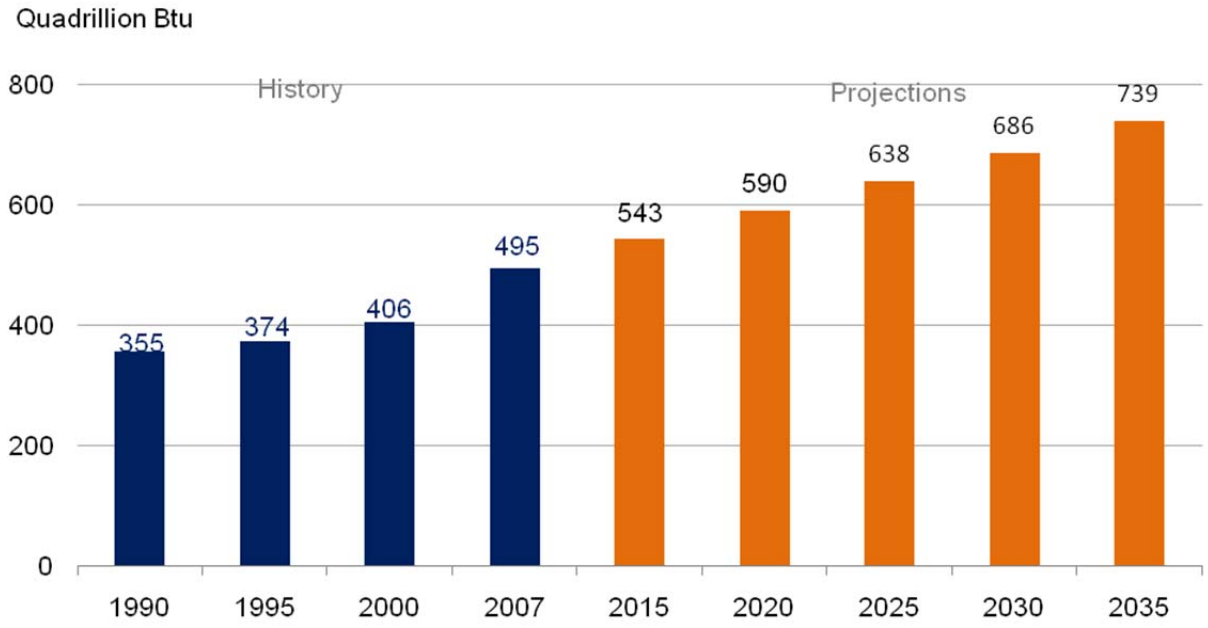

Figure 1.1: World marketed energy consumption, 1990-2035 (1)

[1] 1 quadrillion -BTU of electricity per year = 33.5 x 10^6 kW per year x (365 days per year x 24 hours per day) = 293.5 x 10^9 kW-hrs = 293,500 GW-hrs

Electricity is the world's fastest-growing form of end-use energy consumption as cited in reference (1). Net electricity generation worldwide rises by 2.3 percent per year on average from 2007 to 2035, while total world energy demand grows by 1.4 percent per year. The growth in electricity generation is a consequence of rising standards of living, increase demand for home appliances and the expansion of commercial and residential services. Coal still provides and will continue to provide the largest share of world electricity generation. It accounted for 42 percent of total electrical generation in 2007, and its share is largely unchanged through 2035 (Figure 1.2). The combustion of coal, however, adds a significant amount of carbon dioxide to the atmosphere per unit of heat energy, (2) more than does the combustion of other fossil fuels[2]. In contrast, liquids, natural gas, and nuclear power all lose market share of world generation over the course of the projection period, displaced by the strong growth projected for renewable sources of generation. To satisfy the growing demand, the reference (1) predicts a sharp increase in the utilization of coal over the next 20 years, as well as a steep increase in the development of renewable energy sources as viable solutions to the demand.

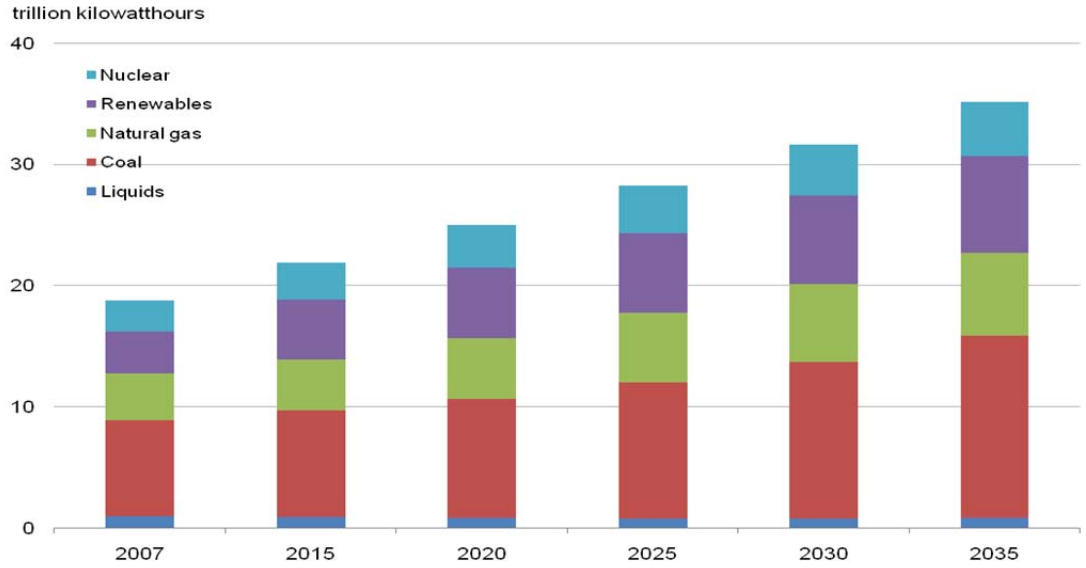

Figure: 1.2 World electricity generation by fuel, 2007-2035 (1)

[2] Coal combustion emits almost twice as much carbon dioxide per unit of energy as does the combustion of natural gas, whereas the amount from crude oil combustion falls between coal and natural gas.

In addition to the above, the world will shortly come to an end of fossil fuels as the world's primary energy resource. With daily consumption of 86.7 million barrels in 2010, and with a 2% annual increase in consumption oil might run out in the near future within 40-50 years. The other forms of fossil fuels have a finite lifetime as our major source of energy, and current forecasts suggest that alternatives must make a major contribution in the near future.

1.2 ENVIRONMENTAL ISSUES

Tied with the increasing energy demand and shortage of fossil fuel supply is the issue of global warming and climate change, caused by burning of fossil fuels. The United Nations' Intergovernmental Panel on Climate Change (IPCC) report Climate Change 2007 (3): This report identified long-lived green-house gases (GHGs) as the main factor affecting global warming and the radiative forcing of the climate system, and pointed out that global GHGs emissions by human related activities have increased 70% between 1970 and 2004. Between 1970 and 2004, global emissions of CO_2, CH_4, N_2O, HFCs, PFCs and SF6, weighted by their global warming potential (GWP), have increased by 70% (24% between 1990 and 2004). The emissions of these gases have increased at different rates; CO_2 emissions have grown between 1970 and 2004 by about 80% (28% between 1990 and 2004) and represented 77% of total anthropogenic GHG emissions in 2004. The largest growth in global GHG emissions between 1970 and 2004 has come from the energy supply sector (an increase of 145%) and combustion of Fossil fuel (3). Some of the impacts of the ongoing climate change has been already observed, these include more frequent occurrence of storms and flooding, alterations in disturbances of forests due to fires and pests, excess heat-related mortality in Europe, changes in infectious diseases vectors, earlier greening of vegetation in the spring, and others. Greater negative impacts, such as decreases in the biodiversity and productivity of crops, increase in risk for coastal erosion due to sea-level rise, and an increase in malnutrition are projected if the current GHG emissions trends (and as a result, the trend in globally increasing temperature) continue in the next 50-100 years. Of all the available technologies producing

renewable energy, sun energy is a hot topic in current research. The following chapter will deal with sun as the main source of energy. After a brief description of the sun, and its energy source it will give a discussion on the quantity, availability and distribution of solar energy worldwide. This chapter will end then with my motivation and outline of the dissertation.

1.3 THE SUN AND ITS ENERGY

1.3.1 Description of the sun

The sun is located at the center of the solar system and provides energy to all planets. Earth obtains its main energy in the form of light and heat from the Sun. The sun's shape as it recently appeared in photos by NASA (4) (see figure 1.3) is almost perfectly spherical. It has a diameter of about 1.4 million km, nearly 10 times that of the largest planet, Jupiter, and 100 times that of Earth. Its radius is 695 500 kilometers. The sun has a total mass of about 2×10^{30} kilograms, at present about 75 % of the Sun's mass consists of hydrogen, while the rest is helium and less than 2% consists of heavier elements, including oxygen, carbon, neon, iron, and others (5). This changes slowly over time as the Sun converts hydrogen to helium in its core.

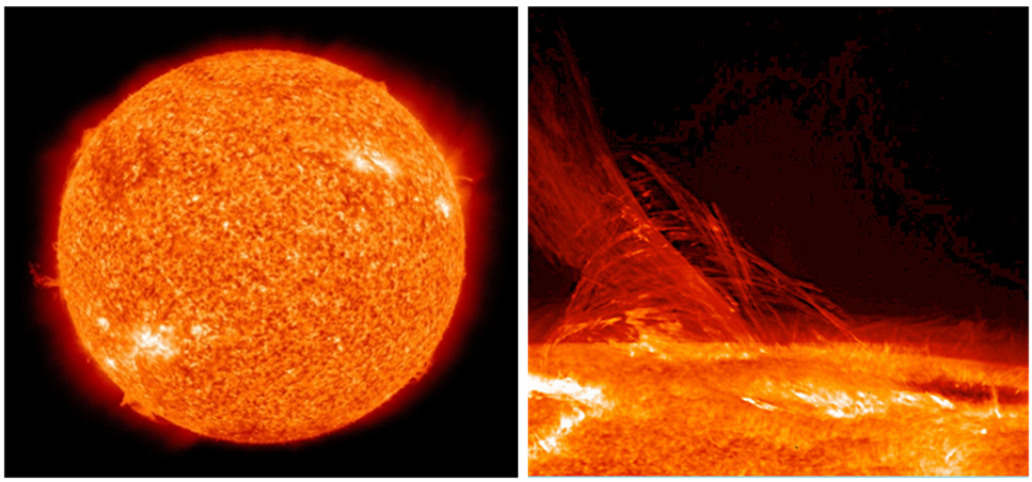

A B

Figure: 1.3 A-The Sun chromospheres is a thin "layer" of solar atmosphere between the visible surface, photosphere, and corona. B- Plasma of the Sun Taken by Hinode's Solar Optical Telescope on Jan. 12, 2007, by NASA

1.3.2 The energy source of the Sun

The sun is an inexhaustible (or at least very slowly exhaustible) source of energy mostly composed of gases. It can be thought of it as one huge thermonuclear reactor, emitting energy into space in the form of electromagnetic radiation. The current stellar classification, has given the sun a spectral class label of G2V. G2 indicates its surface temperature, and V signifies that the Sun is a main sequence star, and therefore generates its energy by nuclear fusion (6). The exact nuclear process is not well known, but the most likely is one by which hydrogen, the Sun's most abundant fuel, is converted to helium by nuclear fusion. It is believed that the sun convert more than 700 million metric tons of hydrogen to about 695 million metric tons of helium each second. In this process of nuclear fusion, huge amounts of energy in the form of electromagnetic rays are released. Most of this electromagnetic radiation emitted from the sun's surface received by Earth surface lies in the visible band centered at 500 nm (1 nm = 10^{-9} meters) Figure (1.4), although the sun also emits significant energy in the ultraviolet and infrared bands, and small amounts of energy in the radio, microwave, X-ray and gamma ray bands.

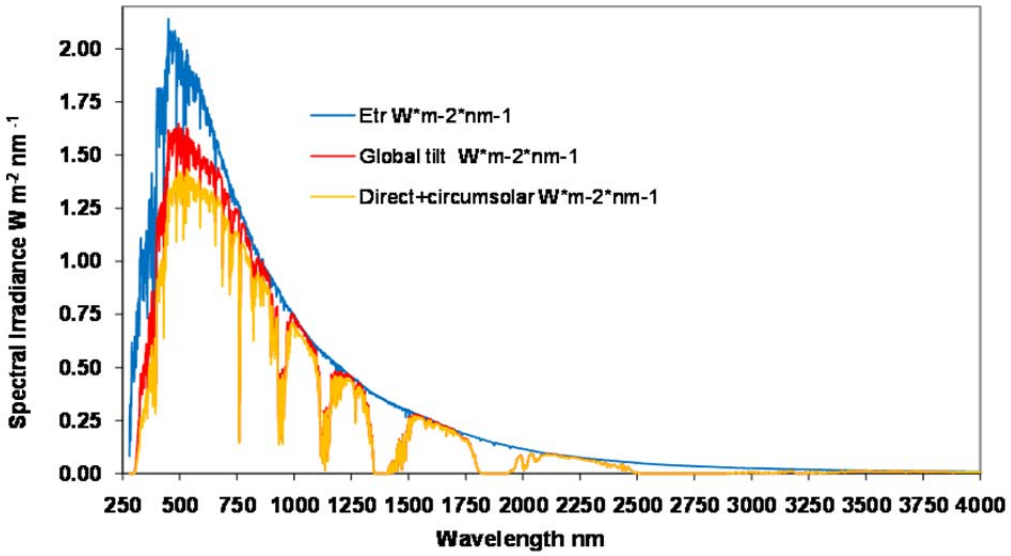

Figure: 1.4 ASTM G173-03 Reference Solar Spectra on Earth (7)

1.3.3 Total quantity of the Sun's energy

The total quantity of energy emitted from the sun's surface in all directions is a quantity known as solar luminosity. This quantity can be approximated by Wien's law and the Stefan-Boltzmann law that describe the peak wavelength and the total radiation power emitted by an object with a certain temperature. Wien's Displacement law tells how to estimate the temperature of a star if we know the wavelength of its maximum emission that can be obtained from the spectral observations of the star.

$$\lambda \text{ max} = 0.0029 \text{ Km/T} \qquad \text{Eq.(1.1)}$$

λ max: Wavelength of maximum emission of the object (in meters)

T: Temperature of the object (in Kelvin)

The maximum intensity of sunlight is roughly at 500 nm = 5.0×10^{-7} m (see graph 1) accordingly using Wien's Displacement law the Sun surface temperature can be estimated as

$$T = 0.0029 / 5.0 \times 10^{-7} \text{ m} = 5800 \text{ K} \equiv 5527 \text{ Ċ}$$

The luminosity of a blackbody (which most stars closely approximate) of temperature T and radius R is given by the Stefan-Boltzmann Law: $L=4\pi R^2\sigma T4$ Eq. (1.2)

Where σ is the Stefan Boltzmann constant ($5.67 \times 10{-}8$ W/m2/K4)

The Stefan-Boltzmann law states that a blackbody radiates electromagnetic waves with a total energy flux F at the surface of the star directly proportional to the fourth power of the Kelvin temperature T of the object:

$$F \text{ surface} = \sigma T4 \qquad \text{Eq. (1.3)}$$

F = Energy flux, per square meter of surface per second

σ = (Stefan-Boltzmann constant) = 5.67 x 10-8 W m-2 K-4 or = (1.3x10-23 J/K)

T = Object's temperature, in Kelvin

The surface area of a spherical object like the sun = $4\pi R2$ Eq. (1.4)

R= the radius of the star.

To calculate the total luminosity of a star we can combine equations 2 and 3 to give:

$F = 4\pi R2\sigma T4$ (W/m2) Eq. (1.5)

The radius of the sun RS ≈ 696000 km, or 696000000 m and its surface area, AS = 4 RS^2 = 6.08 $\times 10^{18}$ m^2. The outward irradiative energy flux (per unit area) at the sun's surface (T ≈ 5800K) is

$\sigma T4 = (5.67 \times 10^{-8}) \times (5800) \times 4 = 7.35 \times 10^7$ W m^{-2} . The total irradiative energy output of the Sun is $7.35 \times 10^7 \times 6.08 \times 10^{18}$ $m^2 \approx 3.87 \times 10^{26}$ W

1.4 SOLAR ENERGY INTERCEPTED BY EARTH

1.4.1 Solar constant

The sun emits some amount of total energy from its surface every second (this is the luminosity of the sun). As that energy is radiated away from the sun, it passes through increasingly larger spherical areas. Since the total amount of energy passing through each sphere is the same, the energy per unit area decreases as the square of the distance (or the square of the radius of the big sphere) from the sun. It is often more convenient to consider the irradiative energy per cross-sectional unit area that the Sun provides for Earth system. This quantity is called the "Solar constant" abbreviated as S_O, and is simply the total energy output of the sun divided by the area (ASE) of the "big sphere".

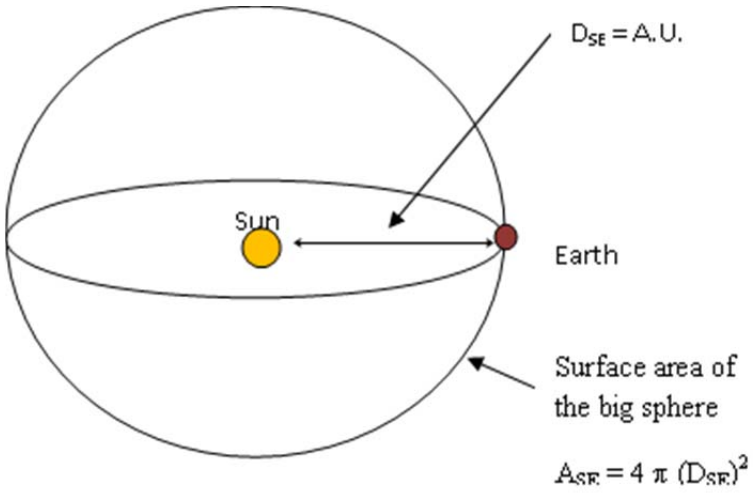

Illustration: 1.1 Calculation of Solar constant

Due to the Earth's elliptical orbit, the actual distance between Earth and Sun varies from a minimum of 147.097.000 km to a maximum of 152.086.000 km (8). For computing the value of the solar constant, the astronomical unit AU is used[3].The astronomical unit is the principal unit of measurement or average earth-sun distance is used. The big sphere centered at the Sun with a radius of D_{SE} (see illustration 1.1) has the total surface area of $A_{SE} = 4\times(D_{SE})^2 = (2.81 \times 10^{23}\ m^{-2})$. The energy output of the sun, 3.87×10^{26} W, is uniformly distributed on this sphere surrounds the sun see illustration (1.1). Therefore the solar constant is equal $So = (3.839 \times 10^{26}\ W)/ 2.81 \times 10^{23}\ m^{-2} = 1377\ W\ m^{-2}$.

[3] AU, mean distance between the earth and sun; one AU is 149,604,970 km (IAU 2009).

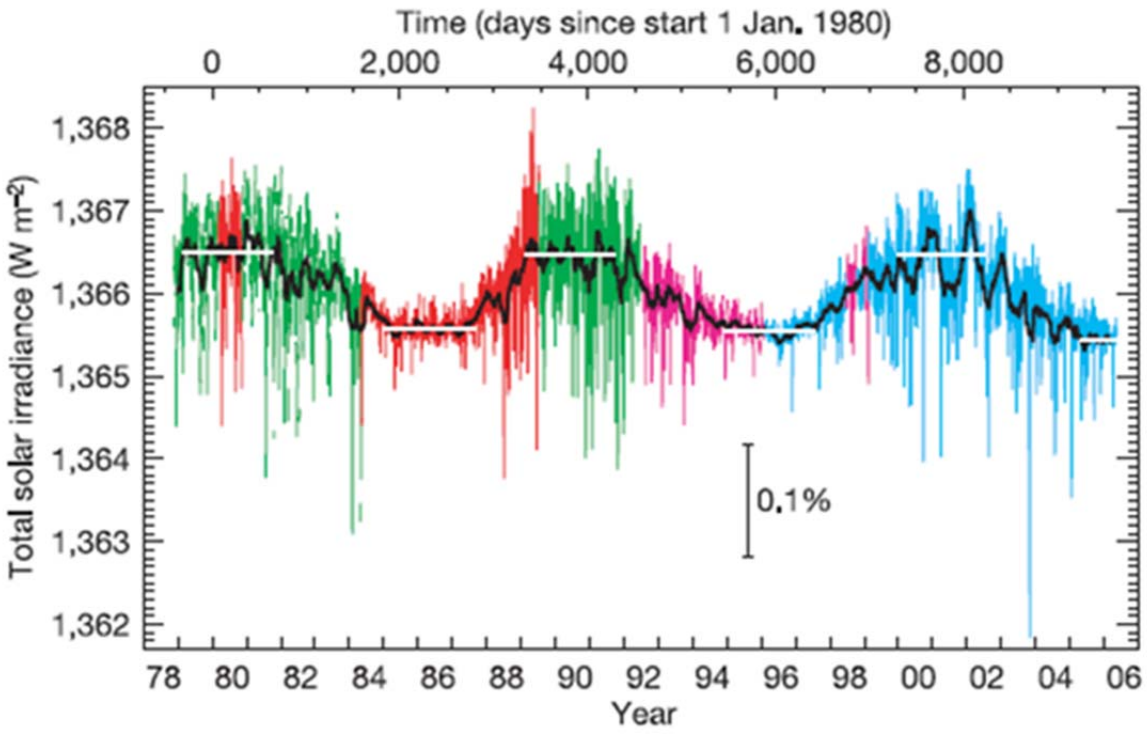

Figure: 1.5 temporal variation of total solar irradiance, as measured by radiometers on several spacecraft from 1978 to 2006 adopted from (9).

Measurements of the solar irradiance by radiometers at spacecrafts on top of Earth atmosphere show the same results of solar constant. The solar constant actually varies by about 0.3% over the 11-year solar cycle (See figure 1.5) but averages about 1,377 W/m^2. This is the solar spectrum we receive outside the Earth's atmosphere that is also known as extraterrestrial or Air Mass 0 (AM0) spectrums.

1.4.2 Insolation: Solar Radiation Striking the Earth Surface

The amount of solar energy that actually passes through the atmosphere and strikes a given area on the Earth surface over a specific time varies with latitude, the seasons as well as with the weather condition and is known as the insolation (incident solar radiation). When the Sun is directly overhead the insolation, that is the incident energy arriving on a surface on the ground perpendicular to the Sun's rays, is typically 1000 Watts per square meter (10). This is due to the absorption of the Sun's energy by the Earth's atmosphere that dissipates about 25% to 30% of the radiant energy (10).

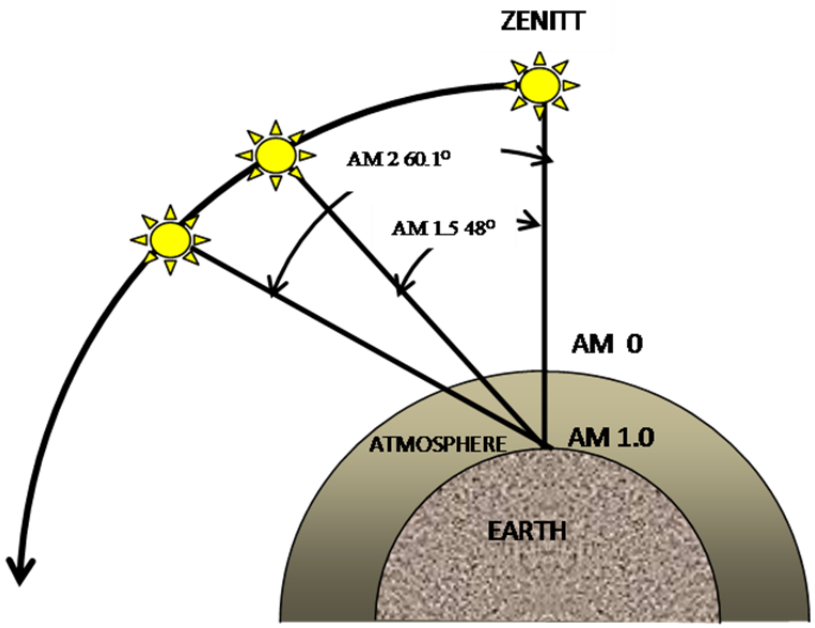

Illustration: 1.2 the path length of the solar radiation through the Earth's atmosphere in units of Air Mass AM

The Air Mass is the path length which light takes through the atmosphere normalized to the shortest possible path length (that is, when the sun is directly overhead). The path length of the solar radiation through the Earth's atmosphere, changes with the zenith angle. It increases from unity for 0^o (zenith) to 1.5 for 48^o and 2.0 for 60^o. The AM1.5 spectrum is the preferred standard spectrum for solar cell efficiency measurements in the literature (11). It quantifies the reduction in the power of light as it passes through the atmosphere and is absorbed by air and dust.

1.4.3 World distribution of solar radiation

Solar radiation is unequally distributed all over the world, and it varies in intensity from one geographic location to another depending upon altitude, which is associated with latitude and season, and atmospheric conditions, which are determined by cloud coverage and degree of pollution. The following guidelines are useful for the broad identification of the geographic areas with favorable solar energy conditions in the world based on the collection of the direct annual average ground solar energy component of sunlight from 1983-2005 (12).

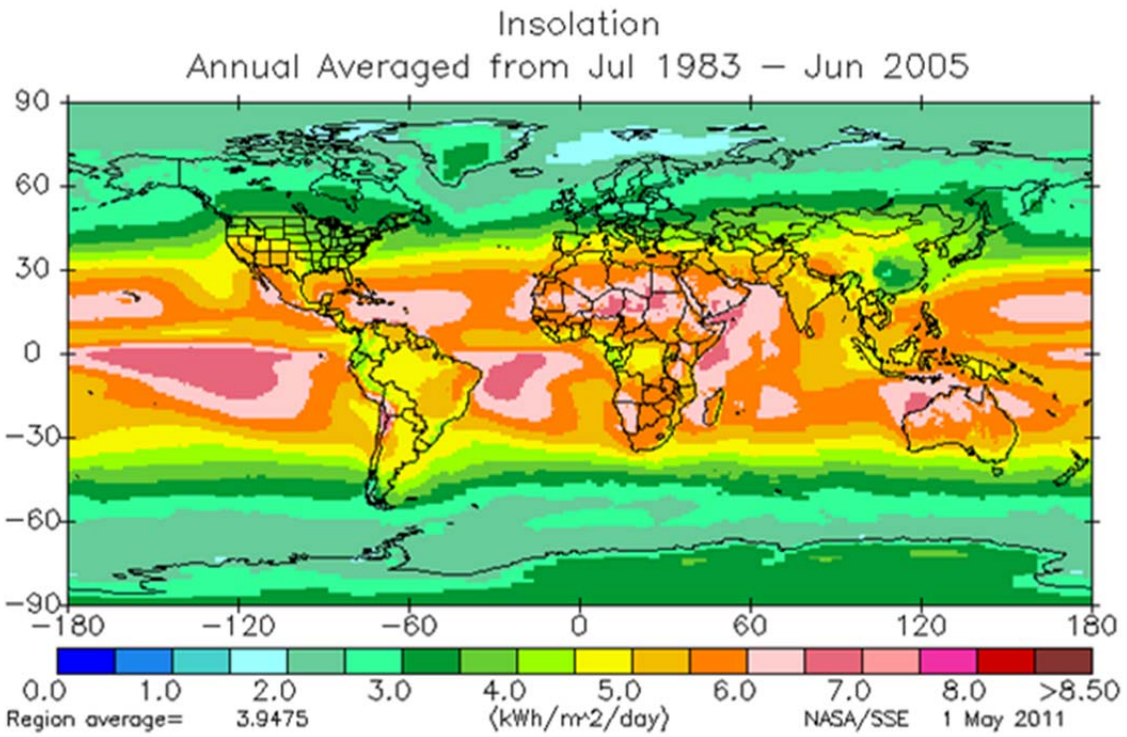

Figure: 1.6 Annual global average insolation from July 1983- June 2005 (12)

The most favorable belt (15-35° N) covers many of Northern African Nations and Southern parts of Asia. It has over 3 000 h/year of sunshine and limited cloud coverage. The Solar insolation in this region averages between 6.5-7.5 KWh/m^2/day (NASA 2011). Because of its geographical location more than 90% of the incident solar radiation comes as direct radiation. The equatorial belt located between (0-15° N), is moderately favorable because, it has high atmospheric humidity and cloudiness that tend to increase the proportion of the scattered radiation. Sunshine is estimated at 2500 h/year with solar insolation between 5.0-6.5 KWh/m^2/day. The less favorable belt is the region between (35-45° N). The scattering of the solar radiation in this belt is significantly high because of the higher latitudes and lower solar altitude. In addition, cloudiness and atmospheric pollution are important factors that tend to reduce sharply the solar radiation intensity. Solar insolation in this region is between 4.0-5.0 KWh/m^2/day. Regions beyond 45° N have less favorable conditions for the use of direct solar radiation, because

almost half of it is in the form of scattered radiation, which is more difficult to collect for use. This limitation, however, does not strictly apply to the potentials for solar UVR applications. In the Southern hemisphere there are three zones of high radiation; in south America, again on the western coast, moving from latitude 10 S to 30 S; in South Africa, between 10 and 35 S; and in Australia, between 15 and 30 S.

1.5 THE MAGNITUDE OF SOLAR ENERGY ON EARTH

To get an idea of how much energy is supplied by the sun one can compare the average amount of sun power received at Earth surface per square meter to the whole world electrical energy consumption. The total amount of energy that is intercepted by the earth at any given moment equals to solar constant times Earth's cross-sectional area facing the sun, $Ac= \pi d^2/4$, where d is the earth diamter. Since the Earth rotates around its axis every 24 hours as it rotates, no energy is received during the night and the Sun's energy is distributed across the Earth's entire surface area of a sphere of $\pi \times d^2$, so that the average insolation is only one quarter of the solar constant or about 342 Watts per square meter. From this amount 23 % is absorbed by dust and other atmospheric gasses and 29% reflected back to space and 48% reaches the surface. Therefore, an average amount of sun power received at Earth surface per square meter is $0.48 \times 342 = 163$ W/m^2. Multiplying this amount by Earth's entire surface area of 5.10×10^{14} m$^2 \times 163$ W/m$^2 = 8.31 \times 10^{16}$ Watts or 83100 TeraWatt. Integrating this power over the whole year the total solar energy received by the earth will be: 83100 TW X 24 X 365 = 727956000 TeraWatthours (TWh)[4].

To put this into perspective, the total annual electrical energy consumed in the world from all sources in 2009 was 17,480 TWh (see figure 1.2) (1). Thus the available solar energy is over 4,0000 times the world's electricity consumption. The solar energy must certainly has to be converted into

[4] Tera Watt Hour means getting power at a capacity of 1 terawatt (10^{12} watts) for one hour

electrical energy, but even with low conversion efficiency of only 8% the available energy will be 58236480 TWh or over a 3331 times the consumption.

1.6 MOTIVATION

A photovoltaic solar cell is a proven technology to capture the solar energy and provides clean and renewable electrical energy that can reduce the world's dependency on fossil fuels, and reduce GHG emission, global warming and other related environmental issues. In spite of the substantial growth over the past decades the high cost of photovoltaic solar cells has remained a limiting factor for the implementation of solar electricity in a large scale. More rapid and widespread implementation of photovoltaic electricity generation requires more advanced technological developments. In particular, technological innovations that reduce the cost of photovoltaic electricity substantially could drive a rapid expansion in implementation of photovoltaic technology.

Currently, the dominant photovoltaic technology is based on solid-state pn junction devices, in which semiconductor absorbers produce electron-hole pairs and the electron-hole pairs are separated by a built-in electrical field in the pn junction to generate electricity. The main semiconductor absorbers used in solid-state solar cells include polycrystalline silicon, (13) amorphous silicon, (14) cadmium telluride (CdTe), (15) and copper indium gallium diselenide Cu (In, Ga) Se2, (16) etc. These types of solar cells have high power conversion efficiency; however, suffer from high manufacturing and material cost.

Among the material systems currently of interest for this reason are the group of molecular-based materials combinations often referred to as 'organic' or 'molecular' photovoltaic materials. These refer to conjugated molecular species, such as polymers, molecules and dyes, which are capable of absorbing light and conducting charge and thereby acting as organic semiconductors (17). Their attraction lies primarily in the possibility of processing such materials directly from solution, and so with bulk synthesis of the chemical materials and bulk solution processing of photovoltaic modules, the cost of the

photoactive material could fall by an order of magnitude compared even with thin film inorganic semiconductors (18), (19). Additionally, the less challenging manufacturing environment, compared, for example, with crystalline silicon wafer production, promises to reduce the capital cost for production facilities and to make the technology more widely accessible, especially in developing countries (20). Moreover it is also believed that if such materials are naturally synthesized and stable the cost could be further reduced.

Dye sensitized solar cell (DSSC) is one of the low cost alternatives for the conventional pn junction based solar cells, and this device is commercially promising because it can be made from low-cost materials and does not require elaborated manufacturing facilities. At the moment there are three types of dyes (21) that can produce cells with AM1.5 conversion efficiencies over 10%. However, these types of dye suffer from the drawback that they are based on the rare ruthenium transition metal.

Asphaltene is one of these materials that for sure fulfill the requirements of organic semiconductors; i.e. absorbing a broad range of visible and near infra red light (22) (23) capable of conducting charge (24), stable and naturally abundant. Asphaltene is an organic moiety that contains a large number of structures, in particular high molecular weight fused aromatic hydrocarbons components with hetero-atoms (25). Most of the researchers have found that the sign of asphaltene charge is positive in organic solvent such as heptane, toluene, ethanol, and nitro methane as studied by zetametry (26), and electrophoresis (27). The origin of the electric charges is a consequence of an electron transfer between the organic solid particles and the liquid organic phase (24).

Asphaltene therefore is an excellent candidate for use in DSSC. Despite of the long term research on this material, there has been no any study directed to its potential use in such purpose. The following chapter will bring in a latest literature survey on asphaltene chemical and elemental structure, molecular size and shape, fractionation processes, and some of its physical and optical properties relevant to its proposed use.

1.7 DISSERTATION OUTLINE

Chapter one of this dissertation starts with an introduction to the main world energy related problems; increase energy demand, shortage of energy supply and environmental issues related to combustion of fossil fuel. The Sun description, its energy source, total quantity of the solar energy reaching the earth surface, as well as world distribution of solar energy is then discussed. The chapter closes with an elaboration on the magnitude of solar energy on earth, the importance of capturing this energy and problems of wide scale implementation of photovoltaic solar cells on earth. Chapter two is intended to give the reader an overview on asphaltene, its chemical composition, molecular weight and shape, and physical properties as well as methods of its fractionation. The history of photovoltaic cells, their status, its development, and trends in the photovoltaic industry are then discussed in chapter three, which also goes a deep insight into the dye sensitized solar cells in particular it is the main subject of this dissertation. Chapter three starts with a brief abstract of the device's history, the technological ground of its development, its operation principle, and the main cell components; and goes onto materials used in manufacturing it, technical considerations in building it and its characterization parameters; and ends up with ways to improve DSSC performance. Chapter four contains experimental work and discussion of the results obtained. The dissertation then ends with a conclusion and recommendation for future work.

Chapter: 2 Asphaltene

2.1 ASPHALTENE DESCRIPTION

Asphaltene is the part of crude oil that contains a large number of structures, in particular high molecular weight fused aromatic hydrocarbons components with hetero-atoms. Asphaltene usually appears brown to black and the melting point varies with oil geographical sources. Asphaltene decomposes when the temperature exceeds 300-400 °C (28). In view of the complexity of the chemistry, asphaltenes are defined as the portion of crude oil insoluble in light n-alkanes (e.g., *n*-heptane or *n*-pentane), but soluble in aromatic solvents (e.g., benzene or toluene). Asphaltene extracted using *n*-pentane is known as C5-Asphaltenes and with *n*-heptane is known as C7-Asphaltenes. The amount, chemical composition, and molar mass distribution of the Asphaltene "solubility class" vary significantly with the source of the crude oil and with the method of precipitation (29); (30); (31); (32); and (33).

2.2 ELEMENTAL COMPOSITION

As any other hydrocarbons, the primary elemental components of petroleum asphaltene are hydrogen and carbon. Ouchi, in 1985 has shown that H/C ratio is linear function of the portion of aromatic carbons of petroleum fractions, as measured by C^{13}-NMR (carbon nuclear magnetic resonance) (34). The H/C ratios of asphaltene are averaged between 1.1:1 to 1.4:1 (35), and (34). C^{13} nuclear magnetic resonance (NMR) and Carbon K-edge X-ray absorption near-edge spectroscopy (XANES) studies show that about 50 % of the carbon is aromatic, and the rest saturated (36).

The elemental composition of 57 different asphaltenes from 8 countries was reported by Speight in 1991. He found that carbon and hydrogen contents of asphaltene do not vary significantly, however, the proportion of hetero-elements, such as oxygen, sulfur and nitrogen, varies significantly - from 0.3 to 4.9% for oxygen; from 0.3 to 10.3% for sulfur; from 0.6 to 3.3% for nitrogen (37). This observation

suggests that the variation of hetero-element content may be the main contributor to the differences in the physical properties of asphaltene.

2.2.1 Sulfur

Following carbon and hydrogen, sulfur is the third most abundant element found in asphaltene. The average sulfur content of asphaltene varies from 2-6 % but it can be identified at concentration above 10 % (38). Sulfur form identification in asphaltene has been studied by the application of x-ray absorption spectroscopy by George et al., 1990; and by XANES (X-ray Absorption near Edge Structure) spectroscopy (39). The data gave a clear demonstration of the existence of nonvolatile sulfide and thiophene sulfur in the asphaltene with thiophene species are the most dominant. Other forms of sulfur that found to occur in asphaltene include the alkyl–alkyl sulfides, alkyl–aryl sulfides and aryl–aryl sulfides (40); (41).

2.2.2 Nitrogen

Studies on the disposition of nitrogen in petroleum asphaltene indicated the existence of nitrogen as various heterocyclic types (42); (43); (44). Much of the nitrogen is believed to be in aromatic locations (45). There is also evidence for the occurrence of carbazole nitrogen in asphaltene (46) and (47). Application of XANES spectroscopy to the determination of nitrogen species in asphaltene, confirmed the presence of pyrrolic nitrogen and pyridinic nitrogen being the two major types of nitrogen (25). In fact, the technique showed the predominance of pyrrolic nitrogen in the samples examined.

2.2.3 Oxygen

The presence of oxygen in asphaltene is evaluated mainly through elemental analysis (by difference) and by chemical reaction. The total content of oxygen in asphaltene from different sources may vary from 1% to 7% by weight. Oxygen was found to exist in asphaltene as in carboxylic, phenolic and ketonic locations (42), but is not usually regarded as being located primarily in heteroaromatic ring systems.

Some evidence for the location of oxygen within the asphaltene fraction has been obtained by infrared spectroscopy. Examination of dilute solutions of the asphaltene in carbon tetrachloride show that at low concentration (0.01% wt/wt) of asphaltene, a band occurs at 3585 cm^{-1}, which is within the range anticipated for free non-hydrogen-bonded phenolic hydroxyl groups. In keeping with the concept of hydrogen bonding, this band becomes barely perceptible, and the appearance of the broad absorption in the range 3200 to 3450 cm^{-1} becomes evident at concentrations above 1% by weight. Other evidence for the presence and nature of oxygen functions in asphaltene has been derived from infrared spectroscopic examination of the products after interaction of the asphaltene with acetic anhydride. Thus, when asphaltene are heated with acetic anhydride in the presence of pyridine, the infrared spectrum of the product exhibits prominent absorptions at 1680, 1730, and 1760 cm^{-1}. These changes in the infrared spectrum of the asphaltene fraction as a result of treatment with refluxing acetic anhydride suggest acetylation of free and hydrogen-bonded phenolic hydroxyl groups present in the asphaltene constituents (42).

2.2.4 Metal content

Various metals (e.g., Ni, V, Fe, Al, Na, Ca, and Mg) have been shown to accumulate in the asphaltene fraction of crude oil, typically in concentrations less than 1 % w/w (48), (49), (50), and (51). Vanadium and nickel are generally the most abundant of the trace metals, are present mainly as chelated porphyrin complexes, and have been linked to catalyst poisoning during upgrading of heavy oils (52), (53). The concentrations of other trace metals not bound in porphyrin structures (e.g., Fe, Al, Na, Ca, and Mg) have also been reported to vary in deposits as a function of well depth (54), and among asphaltene sub fractions (48), (51).

2.3 STRUCTURE OF ASPHALTENE

Due to the complexity of asphaltene molecules, finding the exact structure of asphaltene has proven to be an overwhelming task. Various techniques have been used to investigate the structure of

asphaltene using physical methods that include infrared spectroscopy (IR), nuclear magnetic resonance (NMR), electron spin resonance (ESR), mass spectroscopy, X-ray, ultra-centrifugation, electron microscopy, small angle neutron scattering, small angle X-ray scattering, quasi-elastic light scattering spectroscopy, vapor pressure osmometry (VPO) and gel permeation chromatography (GPC) as discussed by Ruiz-Morales, and Mullins, 2007 (25).

Although the complete structure of asphaltene has not yet been completely revealed, some common features have been established. Asphaltene are now believed to consist of condensed aromatic rings that carry alkyl and salicylic systems with hetero elements (i.e., nitrogen, oxygen and sulfur) scattered throughout in various, including hetro-cyclic locations (55), (25). The aromatic carbon content of asphaltene is typically in the range of 40 to 60 %, with a corresponding H/C atomic ratio of 1.0-1.2. The NMR results indicate that the average number of rings in a single fused ring system is around 7 (56). In a study conducted by Groenzin and Mullins, 2000, (25), fluorescence depolarization technique was applied to survey the molecular size of a broad range of asphaltene and related compounds. It was found that, the variability in asphaltene molecules is huge, some with nitrogen, others with sulfur, some with a big ring system, others with a small ring system, an occasional molecule with a metal, a porphyrin, etc.

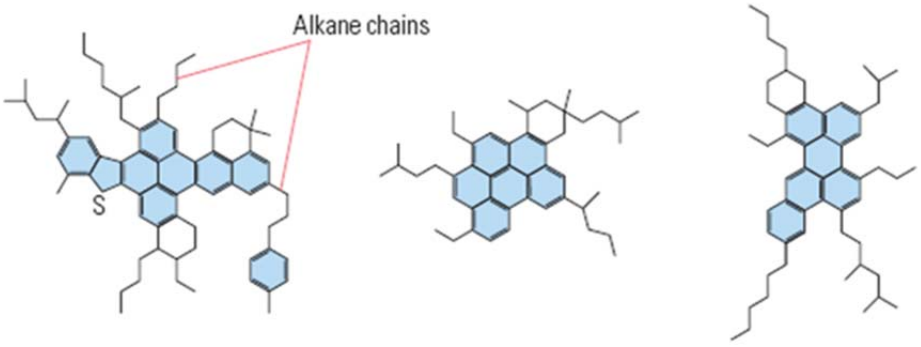

Figure: 2.1 Idealized molecular structure of asphaltene

At the risk of oversimplifying, three idealized asphaltene structures were proposed. These three structures are presented in figure 2.1. Idealized molecular structures for three asphaltene consistent with overall molecular size, aromatic ring systems, and chemical speciation, the aromatic rings are shown with darker lines (57). Asphaltene molecules are shaped "like your hand" with the palm representing the core aromatic ring system and the fingers representing the peripheral alkane substituents (58), (59).

2.4 ASPHALTENE MOLECULAR MASS

The molar mass of asphaltene has been a topic of continued controversy over the last decades mainly due to its tendency to aggregate or associate even at low concentration. However, with the development of more advanced techniques, the debate on molecular mass of asphaltene seems to be over. In the past the molar mass of asphaltene has been measured by various techniques such as Vapor Pressure Osmometry (VPO), mass spectrometry (MS), size exclusion chromatography (SEC), and scattering phenomena such as small angle X-ray (SAXS), small angle neutron scattering (SANS). Molecular mass determined by light scattering methods (SAXS, SANS) and fluorescence depolarization technique differ by as much as factor of 10 or more. It has been understood that many of these techniques have measured molar mass of aggregated asphaltene or micelles than a single asphaltene molecule. Also, it is recognized that the molar mass of asphaltene depends on the technique and experimental condition (time, concentration and temperature) employed for the measurement. Size exclusion chromatography has yielded average molecular weights as high as 10,000 amu (60) . In another study, laser desorption mass spectroscopic results yielded asphaltene molecular weights of 400 amu with a range of roughly 200-600 amu. Fluorescence depolarization measurements indicated the molecular weights of 750 amu with a range of roughly 500-1000 amu (57).

Some obstructions on using MS to measure the molar mass of asphaltene has been the concern that some ionization methods may cause aggregation, fail to ionize some components, or break high-molecular-weight species into smaller pieces. But two recently developed MS methods appear to

alleviate those concerns. Both indicate molecular-weight of asphaltene between 600-1100 amu. The first is two-step laser desorption ionization MS (L2MS), used by Pomerantz, et al, 2008 and coworkers (61). In this technique, an infrared CO_2 laser desorbs species from the surface by heating them enough to pop them off as neutral molecules but not enough to break them apart. An ultraviolet laser ionizes the intact molecules by exciting their aromatic rings, and the fragments are then mass analyzed. The researchers find a molecular weight distribution that peaks around 600 amu and extends to more than 1,000 amu. The second new method is laser-induced acoustic desorption (LIAD), utilized by Shea and coworkers (62). LIAD gets around this problem by evaporating asphaltene as neutral molecules rather than ions. Shea 2007 and coworkers deposit samples on titanium foil and fire a laser at the opposite side. The laser energy is converted to a sound wave that travels through the foil and pushes molecules off the other side. The molecules are then subjected to electron ionization, which non-selectively ionizes all organic compounds; they found a molecular weight of asphaltene ranges from 400 to 1,100 a.m.u. When they compare asphaltene samples from around the world, they find that molecular weight distributions vary depending on geographic origin. For example, Brazilian asphaltene samples have a lower molecular weight range than North American asphaltene.

2.5 ASPHALTENE SIZE AND SHAPE

The asphaltene particle size and shape varies widely in the literature (63) reported that the diameter of disk-like asphaltene entities in tetrahydrofuran for safanya asphaltene fractions is about 13 nm. Rajagopal and Silva in 2004 (64) measured the spherical particle size of asphaltene in toluene by light scattering method and estimated it to be 23 nm even at very low concentration of about 1 ppm. The freeze-fracture-transmission electron-microscopy (FFTEM) technique was employed to study the asphaltene particle diameter in toluene medium and was found to be in the range of 7-9 nm (65). In more recent study conducted by Chianelli et al. 2007 (58) using WAXS wide angle x-ray scattering and SAXS Small angle x-ray scattering on Venezuelan and Mexican asphaltene show the presence of the

"asphaltene particles" with sizes in the range of 3–5 nm. Thus, the survey of the literature indicates that the asphaltene particle diameter varies between 3 and 23 nm. The variation in data is attributed to the difference in solvents, techniques and concentration range employed. The variety of shape of asphaltene has been proposed including thin-disk, spherical, fractal-like, oblate ellipsoid, prolate and discoid (63) (65); (66); (58).

2.6 ASPHALTENE SUB-FRACTIONATION

2.6.1 Sub-fractionation Procedures

Separation of the total asphaltene into sub-fractions is often motivated by an attempt to probe the relationship between the chemical composition, solubility, aggregation behavior, and emulsion-stabilizing properties of discrete portions of the asphaltene fraction. Previous methods of separating asphaltene into sub-fractions include gel permeation chromatography (67), sequential elution solvent chromatography (68), liquid-liquid extraction (69), dialysis fractionation (65) , ultracentrifugation (70), , and precipitation by the addition of flocculants (69), (48), (57), and (51)

2.6.2 Coarse Fractionations

Two different experimental methods are common for the separation of asphaltene into sub-fractions by precipitation and will be referred to as the "coarse" and "fine" fractionation methods. The solvent/anti-solvent combination used and exact procedure for isolation of the precipitated asphaltene generally varies between researchers; however, in both methods the total asphaltene fraction is typically dispersed in a "good" solvent (e.g., toluene) at a fixed solute concentration and a flocculating solvent (e.g., *n*-heptane) is added to induce partial precipitation. During a coarse fractionation, two asphaltenic fractions (i.e., insoluble and soluble) are generated by asphaltene precipitation at a given solvent condition. Typically, the ratio of flocculants to solvent is varied so that several pairs of more and less soluble fractions are generated. For example, Yarranton and coworkers studied the solubility behavior and molar mass distribution from Vapor Pressure Osmometry (VPO), and interfacial tension

measurements of several Athabasca n-C7 asphaltenic coarse fractions precipitated from mixtures of hexane and toluene (71). Andersen and coworkers generated several coarse fractions of Boscan n-C7 asphaltene by precipitation in mixtures of heptane and toluene (69). Spiecker studied the solubility and aggregation behavior by SANS of coarse asphaltenic fractions precipitated from various parent asphaltene by a similar procedure (48). In each of the above studies, the aromaticity and N/C content of the less soluble fractions generally decreased with increasing yield of precipitated asphaltene (i.e., higher flocculent/solvent ratios) and corresponded with an increase in aggregate size. Sulfur and oxygen contents were typically distributed evenly throughout the fractions. Furthermore, the less soluble fractions were generally more aromatic, had a higher N/C content, and formed larger aggregates in toluene and pyridine than the more soluble fractions. The various studies offered differing results concerning the isolation of trace metal species. UV Visible and HPLC-SEC measurements on Boscan asphaltene indicated that metallo-porphyrins were preferentially extracted in the more soluble fraction and contents decreased with decreasing asphaltene yield of the insoluble fraction (69). In contrast, higher concentrations of various trace metals (e.g., Fe, Ni, V, Na) were observed in the less soluble fractions compared to the more soluble fractions as determined by the inductively coupled plasma (ICP) technique (48).

2.6.3 Fine Fractionations

Instead of generating only two fractions, one of which represents at least half of the original asphaltene by mass, the fine fractionation procedure separates the total asphaltene into several discrete sub-fractions by a step-wise increase in the concentration of the flocculating solvent. During each precipitation step, a small amount of asphaltenic material is precipitated and isolated, the soluble filtrate is recovered, and the next fraction is precipitated after a change in solvent conditions. The major difference between the coarse and fine fractionation methods is that the coarse fractions precipitated at higher flocculent contents likely contain the entire subset of chemical species present in fractions

precipitated at lower flocculant contents; whereas each fine fraction should represent the discrete subset of asphaltenes that precipitate between the ranges of two solvent conditions. For example, Yang et al. isolated six asphaltenic sub fractions from Athabasca bitumen by step-wise increasing the ratio of n-heptanes to bitumen (H/B) (51).The first fraction to precipitate was the most aromatic and had the highest concentration of Fe, Ca, Mg, and Al. Atomic H/C ratio was observed to increase and metalloporphyrin contents decrease systematically as the fractionation proceeded (i.e., at higher H/B ratios). Unlike the previous analyses of coarse fractions by SANS and V.P.O. (48) and (72), no significant variations in aggregate molar mass were observed byVapor Pressure Osmometry (VPO), for the fractions dissolved in toluene at 50 C^{o}. Groenzin and coworkers isolated six sub fractions of n-C5 asphaltene by sequential precipitation in mixtures of n-pentane and toluene (73) Fluorescence depolarization measurements on solutions of the asphaltenic fractions in toluene indicated that the less soluble fractions emitted at higher wavelengths than more soluble fractions, suggesting the less soluble fraction possibly contained a higher population of large chromophores. Buenrostro-Gonzalez et al. compared the chemical composition of sub fractions generated by step-wise increasing the amount of flocculants (i.e., acetone or n-heptane) added to a 2.3 % (w/w) solution of Mayan n-C7 asphaltene in toluene (74).Ten discrete fractions were generated for each solvent mixture, but not enough material was precipitated during the first few fractionations (i.e., the least soluble asphaltene fractions) to perform subsequent chemical analyses. There were no apparent trends in atomic H/C, N/C, S/C, or O/C with the order of fractionation for the heptane-toluene fractions analyzed. Similarly, there were no apparent trends in atomic H/C, N/C, or S/C for the acetone-toluene fractions; however, O/C content appeared to increase continuously for the third through sixth fraction. These results suggested that polar interactions dominated the solubility behavior at low acetone contents, while dispersion interactions dominated the solubility behavior at high acetone contents and for the heptane-toluene fractions. Similar polar fractionations were performed by sequentially increasing the amount of n-pentane flocculent to a

mixture of Mobil and Venezuelan n-C7 asphaltene in methylene chloride (50), and (75). Marked differences in physical appearance, crystallinity, and solubility behavior (in dodecylbenzene sulfonic acid) were observed between the most polar and least polar fractions. Similarly, the more polar fractions had higher metals contents (i.e., Fe, Ni, and V) than the less polar fractions.

2.7 ASPHALTENE AGGREGATION

The aggregation mechanism for asphaltene is generally believed to be governed by van der Waals dispersion interactions, electrostatic interactions between molecular charges, hydrogen bonding of polar moieties, and orientation dependent repulsive steric interactions with lesser contributions stemming from intermolecular charge transfer and weak inductive interactions (76). A recent proposal based on a review of the current literature suggests that strong specific forces, such as interactions between polar heteroatoms or π-bonding between aromatic moieties, drive asphaltene aggregation while weaker non-specific dispersion forces dominate asphaltene precipitation (77).

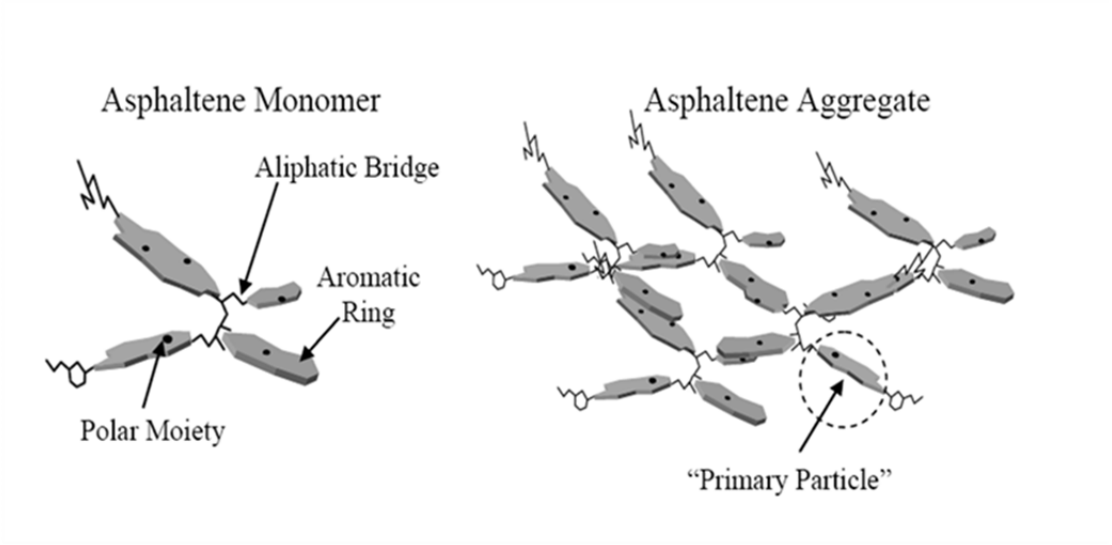

Figure: 2.2 Asphaltene Aggregate Structure

Although the intermolecular interactions that drive asphaltene aggregation are generally accepted, debate still exists over the orientation of heteroatom, alkyl, and aromatic moieties within the molecular framework. For example, two different models have been adopted in the literature to account

for the degree of aromatic condensation within the fused ring backbone of asphaltenes, but both models are consistent with monomer masses between 500 to 1000 amu. One is the so-called “continental” model of asphaltenes (76), which posits a monomer molecular structure consisting of a large, highly condensed aromatic core surrounded by an aliphatic periphery, as inferred from X-ray diffraction and fluorescence depolarization experiments (73), and (59). Interactions of “continental” monomers would likely to form dense-packed aggregates through stacking interactions of the aromatic cores (78), (79). Alternatively, the so-called “archipelago” model (80) was proposed in which individual asphaltene monomers are comprised of clusters of polycondensed groups consisting of 5 to 7 aromatic rings connected by short aliphatic side chains, possibly containing polar heteroatom bridges (81), , (78), (56). The “archipelago” model is supported by chemical and thermal degradation studies which concluded that the extent of aromatic condensation in asphaltene is significantly lower than generally believed (82). Furthermore, molecular simulation studies on a proposed Athabasca asphaltene structure suggested that the presence of long aliphatic bridges gives asphaltene the capacity to fold themselves into a complex three dimensional globular structure with self-similar internal structure (78). If the archipelago like structure is valid, it seems probable that asphaltenic aggregates possess a porous, reticulated microstructure susceptible of entraining significant amounts of surrounding solvent.

2.7.1Critical nano-aggregate concentration

The critical micelle concentrations (CMC) or more recently critical nanoaggregate concentration (The terminology was changed by the asphaltene community from “micelle” to “nanoaggregate”) (83)of asphaltene have been determined using a variety of different methods such as calorimetric titration (84) and electrical conductivity (83). The data for the values of the critical micelle concentration for the asphaltene found by these methods were in the range of 1 to 5 g/L in toluene. Alternating-current (AC) conductivity measurements performed by Eric Sheu and co-workers on asphaltene in solvent showed a break in the conductivity curve at ∼150 mg/L. A very recent publication conducted by (83) confirmed

that the self-association of asphaltene occurred in organic solvents using electrical conductivity. He observed a clear break between two linear regions at a value of 130 mg/ L that is attributed to nanoaggregate formation. `

Chapter: 3 Photovoltaic

3.1 HISTORY OF PHOTOVOLTAIC TECHNOLOGY

3.1.1 The Photovoltaic phenomenon

The discovery of photovoltaic effect was very important event in the history of scientific development because it stimulated scientists to think about light in a different way. The unusual point about the photovoltaic effect is the relationship between the intensity of the light shined on a piece of metal and the amount of electric current produced. Photovoltaic is defined as the direct conversion of sunlight into electricity using the physical mechanism called the photovoltaic effect. The term "photo" comes from the Greek word *phos* which means light and "voltaic," from the Italian scientist Alessandro Volta, referring to electricity. A photovoltaic (PV) cell, also known as "solar cell," is a device that generates electricity when light falls on it.

The Photovoltaic effect phenomenon was first discovered in 1839 by the French scientist Edmund Becquerel (85), who reported a photocurrent when a silver coated platinum electrode was illuminated with white light in an electrolytic solution and connected to a counter metal electrode (strictly speaking this is a photo-electrochemical effect). About thirty years later in 1873 Willoughby Smith discovered the photovoltaic effect in selenium (86). Later on in 1876, William G. Adams observed that illuminating a junction between selenium and platinum also has a photovoltaic effect (87). By that time the first solid state photovoltaic devices were constructed. However, the photovoltaic effect was not fully understood until the development of quantum theory of light and solid state physics in early to middle 1900s. This strange observation was explained in 1905 by physicist Albert Einstein (1879–1955). Einstein hypothesized that light travels in the form of tiny packets of energy, now called photons.

Einstein's theoretical explanation of the photoelectric effect was very important because it provided scientists with an alternative method of describing light (88). In 1918, a Polish scientist

Czochralski discovered a method for mono-crystalline silicon production, which enabled mono-crystalline solar cells production (89). The first silicon mono-crystalline solar cell was constructed in 1941. From the mid 1950s to the early 1970s, PV research and development (R&D) was intended primarily for space applications and satellite power. Under these circumstances, the first fabricated inorganic solar cell was reported by Chapin, Fuller and Pearson in 1954 at Bell Laboratories (90). It was a crystalline silicon solar cell, which converted sunlight into electric current with an efficiency of 6%. As the space program progressed, silicon solar cells became the universal power source for use on space satellites.

3.1.2 Application of Photovoltaic technology on Earth

Throughout the research and development stage of photovoltaic technology for space applications, researchers never considered this technology practicable for mass power production on Earth. Oil and coal fossil fuels were incredibly cheap when compared with electricity production costs of silicon solar cells. It wasn't until the awareness of the environmental harm caused by fossil fuels and, more likely, the energy crisis of the early 1970s in industrialized nations that public and governmental support of photovoltaic energy began to increase significantly (91). As a consequence the establishment of the biggest photovoltaic companies took place between1970-1979. In 1970, Solar Power Corporation was established. Three years later, in 1973, Solarex Corporation was established. At the Delaware University a solar photovoltaic-thermal hybrid system, one of the first photovoltaic systems for domestic application, was developed. A silicon solar cell of US$ 30 per W was produced. In 1974, the Japanese Sunshine project commenced. A year later, in 1975, Solec International and Solar Technology International were established (92).

Many important events in the field of photovoltaic energy occurred in 1980-1990. BP purchased Lucas Energy Systems and entered the solar industry business. Saudi Arabia installed a solar powered seawater desalination system with 10.8 kW peak power in Jeddah. Volkswagen tested a photovoltaic

systems placed on vehicle roofs with 160 W peak powers for vehicle start up. In 1984, a 1 MW photovoltaic power plant began to operate in Sacramento, California. The same year ARCO Solar introduced the first amorphous silicon modules. In 1985, researchers of the University of New South Wales in Australia constructed a solar cell with more than 20% efficiency. BP built a power plant in Sydney and shortly after another one in Madrid. In 1986, ARCO Solar introduced the first commercial thin film photovoltaic module. In 1989 BP got a thin film technology patent for solar cells production.

3.1.3 Organic photovoltaic

The first organic compound in which photoconductivity was observed was Anthracene revealed in the beginning of the 20th century by Pochettino (93) and Volmer (94). 30 years later in the late 1950s and beginning of 1960s the possible use of organic materials as photoreceptors in imaging systems was acclaimed (95). The commercial potential to produce image making machines as well as scientific interest led to increased research into photoconductivity and related subjects. In the early 1960s it was discovered that many common dyes, such as methylene blue, had semiconducting properties (96).

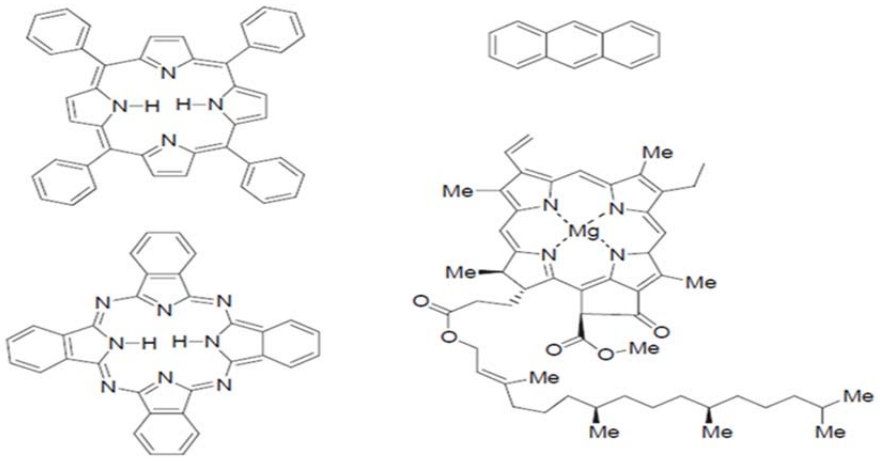

Figure: 3.1 Some of the early investigated organic molecules. Top: TPP and anthracene. Bottom: phtalocyanine and Chl-a.

The first actual organic photovoltaic cell investigations were done on porphyrins and PCS. This class of compounds has remained among the most investigated one, because they are easy to prepare, are

highly colored, have good semiconducting properties and readily form complexes with a number of metal ions. Because of the analogy with natural photosynthetic processes most of the earlier understanding of the organic photovoltaic effect in organic photocells comes from the study of devices fabricated from many biological molecules like carotenes, chlorophylls and other porphyrins, and the structurally related phtalocyanines.

3.2 DYE-SENSITIZED SOLAR CELLS

3.2.1 Historical development

The basis of inventing the DSSC is associated with three main major concepts in technological developments; photovoltaic, sensitization and nano-technology. The historical events of the first one have been already addressed and the following paragraph will focus on the last two. The idea of modifying the band gap of semiconductors to light of wavelength longer than that corresponding to its band gap (sensitization) has been discovered accidently and connected to the beginning of photography dated back to 1873. It was an exciting connection between photography and photo electrochemistry, both of which depend on photo-induced charge separation at a liquid solid interface. Silver halides crystals, first used in photography, have band gaps which range from 2.7 to 3.2 eV, and therefore, these materials are insensitive to wavelengths longer than 460 nm. To make it photosensitive to longer wavelength Vogel in Berlin 1873 (97) associated dyes with the halide semiconductor grains and expand the photo response to longer wavelengths. That was the first film, able to deliver the image of a sight practically into black and white picture. Moser shortly afterward used the same analogy to make the first sensitization of a photo-electrode, (98) and it was confirmed by Rigollot in 1893 (99). However, it took scientists more than 80 years to understand that their operating mechanism is by injection of electrons from photo-excited dye molecules into the conduction band of the n-type semiconductor substrates (100) which was dated from the 1960s. In subsequent years, the idea developed that the dye could function most efficiently if chemisorbed on the surface of semiconductor.

The concept of Nanotechnology on the other hand has been recognized a long time ago and humanity has without knowing employed nanotechnology, in making steel, paintings and durable rubber. Nanotechnology got the biggest boost in the early 1980s with two major developments: the birth of cluster science and the invention of the scanning tunneling microscope (STM). This development led to the discovery of fullerenes in 1985 and the structural assignment of carbon nano-tubes a few years later. In the field of semiconductors, the synthesis, electrical and chemical properties of semiconductor nano-crystals were studied. This led to a fast increasing number of semiconductor nano-particles of quantum dots and nano-structured photovoltaic materials.

The use of dye-sensitization processes in photovoltaic remained rather unsuccessful to develop high efficiency solar cell, until it was combined with nanotechnology and breakthrough at the early 1990's in the Laboratory of Photonics and Interfaces in the EPFL Switzerland. By the successful combination of nano-structured electrodes and efficient charge injection dyes professor Grätzel and his co-workers developed a solar cell with energy conversion efficiency exceeding 7 % in 1991 (101) and 10% in 1993 (102).This solar cell is called the dye sensitized nano-structured solar cell or the Grätzel cell after its inventor.

3.2.2 Operation principle of DSSC

Dye sensitized solar cells (DSSC) or “Grätzel cells” consists of combination of several different materials, every of which performs a specific task toward the overall objective of harvesting solar light and transforming it into electricity (103). A typical DSSC is composed of two sheets of conductive glass. To make it conductive the glass is coated with a transparent conductive oxide layer (TCO). One of the glass plates, the working electrode or the photo-electrode, is covered with a film of porous nano-particles of semiconductor which is sensitized by the dye. The other glass plate, the counter electrode, is coated with a catalyst Pt is commonly used. Both plates are sandwiched together with the help of sealant which also acts as spacer. The electrolyte, commonly a redox couple in an organic solvent, fills the gap

between the two electrodes. When light shines on the cell, the dye molecules absorb photons and become photo-excited. An excited dye molecule injects an electron into the conduction band of the semiconductor and becomes oxidized. The electron then travels through the metal oxide, reaching the collector (TCO). Subsequently, the electron moves through an outer circuit to reach the counter electrode, performing electrical work on the way. The original state of the dye is restored by electron donation from the reduced specie in the electrolyte, completing the circuit. The voltage generated under illumination corresponds to the difference between the Fermi level of the electron in the semiconductor oxide and the redox potential of the electrolyte. Generally the cell produces electric power from light without going through any permanent chemical transformation. However, there are unwanted reactions, which may reduce the overall cell efficiency. These are that the injected electrons may recombine either with oxidized sensitizer or with the oxidized redox couple at the TiO_2 surface, resulting in losses in the cell efficiency (dark current will be discussed latter). The following figure is a schematic representation of the principle of DSSC operation:

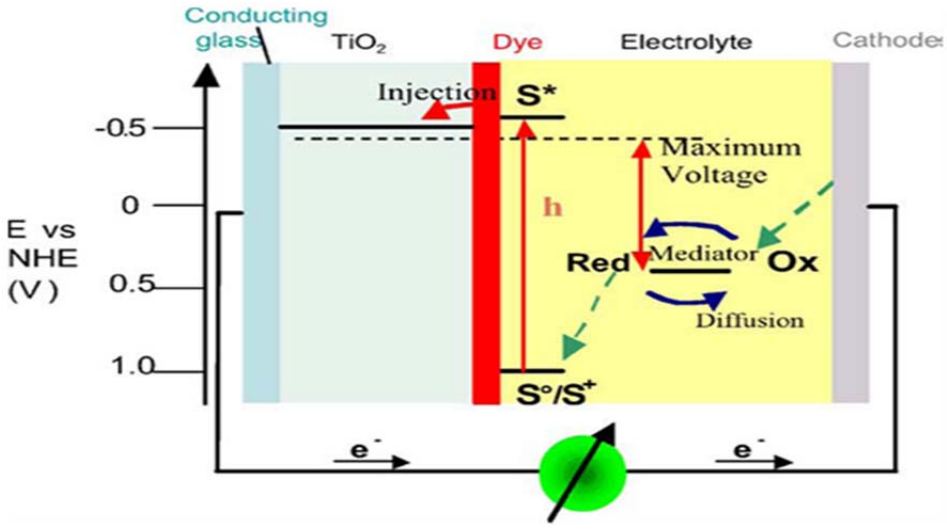

Figure: 3.2 Operation principle of DSSC (104)

3.2.3 Main components of DSSC

3.2.3.1 Conducting substrate

As mentioned above both the working and the counter electrodes in DSSC are made from transparent conductive glass substrate. The most commonly used substrates for DSSCs are made of coated glass with a transparent conducting oxide (TCO). Suitable TCO must have high transparency to most of the electromagnetic radiation as well as high electrical conductivity to efficiently collect all the generated photocurrent. The most widely used TCO, in DSSC is fluorine doped tin dioxide (SnO_2: F or FTO) due to its thermal stability and low cost. Indium tin oxide ($In_2 O_3$: Sn or ITO) has also been used extensively because it has higher specific conductivity. However, because of high cost and limited supply of indium, and the costly layer deposition requiring vacuum, as well as its low stability at higher temperatures alternatives are being sought. Carbon nanotube conductive coatings are a prospective replacement (105).

3.2.3.2 The counter electrode

These conducting glass electrodes has poor reduction ability for I_3^-, therefore a catalyst is highly needed in the counter electrode to overcome the high activation energy of the two electron transfer. Platinum is the most widely used material for this purpose. It acts as a catalyst in the redox reaction at the counter electrode and thus avoiding this process becoming rate limiting in the light energy harvesting system. Platinum however, has another problem apart from its high price, is the non-confirmed possibility of corrosion by the iodide solution, which leads to the formation of PtI_4 (106). Since platinum is very expensive, other cheaper alternatives may take its place like various forms of carbon (107). In this regard, it is found that functionalized graphene sheets with oxygen-containing sites perform comparably to platinum in DSSC (108). Gold, although expensive, is another viable alternative (109) that is constantly used in solid state DSSCs.

3.2.3.3 The working electrode

3.2.3.3.1 Semiconductors

Semiconductors that have narrow band gaps and absorb visible light efficiently are subject to photo-corrosion and therefore are not suitable for DSSC. Metals oxides on the other hand, such as titanium or niobium have a wide band gap, an absorption edge towards the ultraviolet and consequently are insensitive to the visible spectrum. For this reason, the sensitizer, or the dye is adsorbed onto the semiconductor's surface expanding the absorption spectrum range, and thus increasing light harvesting efficiency (110).

Since the beginning of research, TiO_2 has been the preferred semiconductor in DSSCs, in spite of some promising properties offered by other metal oxides such as ZnO (111), SnO_2 and Nb_2O_5 (112). TiO_2, the white pigment, is chemically inert, has good thermal stability non-toxic, relatively cheap, readily available material, and serves as an attractive candidate for many industrial applications (paints, paper, coatings, plastics, etc. (113). Anatase is the most preferred form among the three common crystalline polymorphs of TiO_2 (Rutile, Anatase and Brookite) (113) because it has a high band gap energy (3.2 eV, and absorbs only below 388 nm) making it invisible to most of the solar spectrum, reducing the recombination rate of photo-injected electrons. Rutile has also been employed; however, it has a smaller band gap (3.0 eV) and so is less effective, since photon excitation within the band gap generates holes that act as oxidants making it less chemically stable (114).

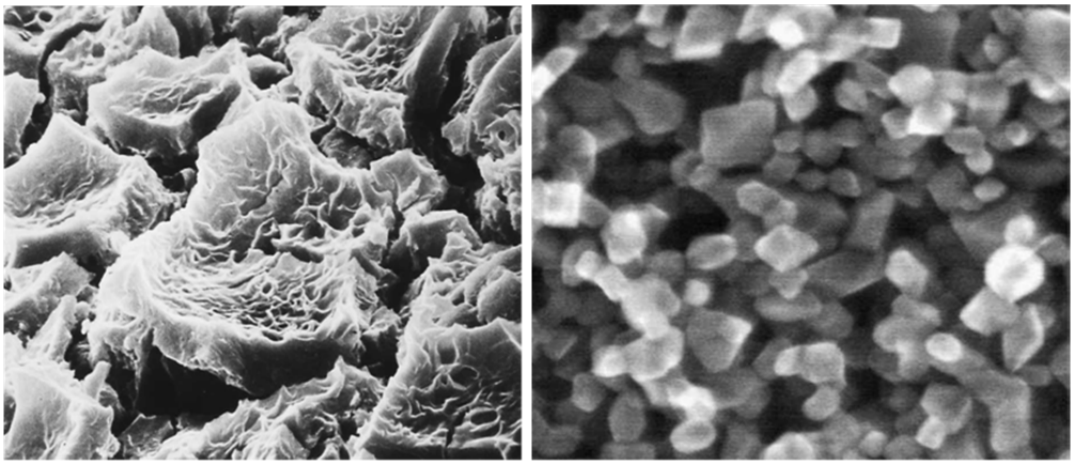

A B

Figure: 3.3 A- scanning electron microscope picture of the fractal TiO2 film used in the first embodiment of the DSSC in 1988. B- Scanning electron micrograph of a TiO2 anatase colloid film (104)

The TiO_2 film morphology plays an important role in the DSSCs performance. In order to obtain the maximum area available for dye adsorption using the minimum quantity of TiO_2, the semiconductor layer should have nanostructure mesoscopic morphology (Figure: 3.3 B) essential for a high specific surface area. A monolayer of dye on a flat surface absorbs at most a few percent of light because it occupies an area that is much larger than its optical cross section. In the first laboratory embodiment of the DSSC which dates back to 1988 (115), the photo-anode was a titanium sheet covered with a high surface area "fractal" TiO_2 film that had a roughness factor of about 150. The overall conversion efficiency in full sun light by that DSSC had an conversion efficiency in between 1% and 2%.Years later, in 1991 Grätzel reported a breakthrough, with an efficiency of around 7% achieved by the innovative use of a nano-scopic TiO_2 particle layer that produces a junction of huge contact area. The semiconductor's surface is thus enlarged over 1000 times allowing for efficient harvesting of sunlight by the adsorbed monolayer of sensitizer.

At the beginning, it was thought that the meso-porous films could elevate charge carrier recombination. However, this does not happen, because the injected electron and the positive charge find themselves on opposite sides of the liquid-solid interface within picoseconds after light excitation of

the dye (116). Nevertheless, since the injected electron has to move across a large number of colloidal particles and grain boundaries, there will be an increased probability of recombination with increased film thickness. Thus, there exists an optimal thickness to obtain maximum photocurrent. In addition, Zhu *et al*. observed that recombination occurs close to the glass coated with a TCO layer and not throughout the entire Titania matrix. For this reason, present researchers use a compact (117) or nanocrystalline TiO_2 as "blocking layer". The use of a light-scattering layer is also quite common; it consists of larger Titania particles that work as a photo-trapping system (118).

Typical semiconductor film thicknesses are 5-20 μm, with TiO_2 mass of about 1- 4 mg cm^{-2}, film porosity 50-65%, and average pore size 15 nm and particle diameters of 15-20 nm. The three deposition techniques commonly used to deposit the semiconductor onto the glass substrate are screen-printing doctor blading, and spin coating (117). A relatively new and exciting research field in semiconductor morphology is the use of nanostructures, namely nanotubes, nanowires, and nanorods (119) and - (120).

3.2.3.3.2 The sensitizer

Despite the fact that the highest efficiency of the dye sensitized solar cells has been achieved from a collaborative effect of numerous physical-chemical nanoscale properties, the key issue is the principle of dye sensitization of large band-gap semiconductor electrodes. In the dye sensitized solar cells this is accomplished by coating the internal surfaces of porous TiO_2 electrode with special dye molecules tuned to absorb the incoming photons (104). The dye is the light absorber and the photoreceptor sensitizing the semiconductor and so some conditions must be fulfilled. Without a doubt a dye that absorbs nearly all the sunlight radiation incident on earth, like a black-body absorber is highly desirable. The solar spectrum has its best or greatest possible intensity in the IR region (ca. 1200 nm) (see figure 1.4) and so it is required to shift the absorption peak of the dye to as low energy as possible. On the other hand, the energy content of the photon decreases as one move further into the IR region, so 920 nm has been chosen as the threshold wavelength below which the sensitizer should absorb (113).

In addition to that, the dye should be chemically absorbed into the surface of the semiconductor, so it must carry groups to attach the dye to the surface, such as carboxylate (121), (122) or phosphonate, (123) and (124) groups, being these the most employed ones. Other groups, like boronic acid (125), salicylate (113), silanes (126) amides (127), ethers (128) or hydroxamic acid groups (129) can also be employed to attach photo-and redox-active molecules to metal oxide surfaces. Upon excitation the dye should inject electrons into the solid semiconductor with a quantum yield of unity, and this is best done when the electronic coupling of the donor levels of the dye and the acceptor levels of the semiconductor are well matched. The energy level of the excited state of the dye should be lower than the conduction band of the oxide to minimize energetic losses during the electron transfer reaction. It is also important that the redox potential of the sensitizer should be sufficiently positive than it can be regenerated via electron donation from the redox mediator (130).

Finally, the sensitizer should be stable enough to carry on about 10^8 turnover cycles corresponding to about 20 years of exposure to natural light (131). In order to achieve that, one has to make sure that the electron injection and the recovery of the oxidized form by the redox couple are fast enough to suppress side reactions like degradation (e.g., loss of ligand), desorption or aggregation. To date, the best photovoltaic performance both in terms of conversion yield and long-term stability has been achieved with polypyridyl complexes of ruthenium (II) what so called N3 and Black dye (see figure) (131).

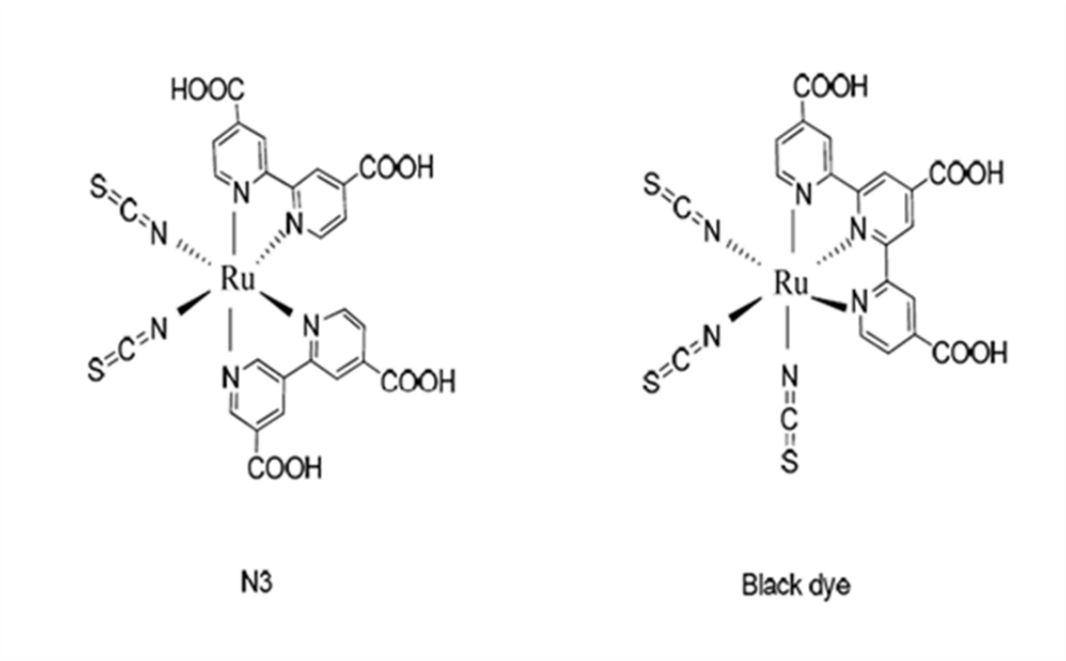

Figure: 3.4 Chemical structure of the two of ruthenium complexes N3 and Black dye (131).

Despite the high performances of these two dyes, other non-metallic alternatives are currently being pursued (132). Due to its scarcity, ruthenium is a very expensive metal and hence the necessity for alternative is required. The most promising alternatives are natural organic dyes, which are considerably cheaper, though so far generally less stable and less efficient. However, they have a great potential for this application due to their high absorption coefficients compared to ruthenium sensitizers (133).

When talking about organic dye, the most two organic dye structures that attract particular attention are porphyrins (134) and phtalocyanine (135), the former because of the analogy with natural photosynthetic processes, the latter because of their photochemical and phototherapeutic applications. However, porphyrins lacks red light and near IR absorption so it cannot compete with the N3 or "black dye" sensitizers. Phtalocyanine in contrast show intense absorption bands in this spectral region. However, its problem is the unsuitable energetic position of the LUMO level which has turned out to be difficult so far (104). A significant progress in the use of organic dyes for DSSCs was made by the

group of (136), (137).They used coumarine or polyene as sensitizers (see figure 7), and got high solar to electric power conversion efficiencies reaching up to 7.7% in full sunlight.

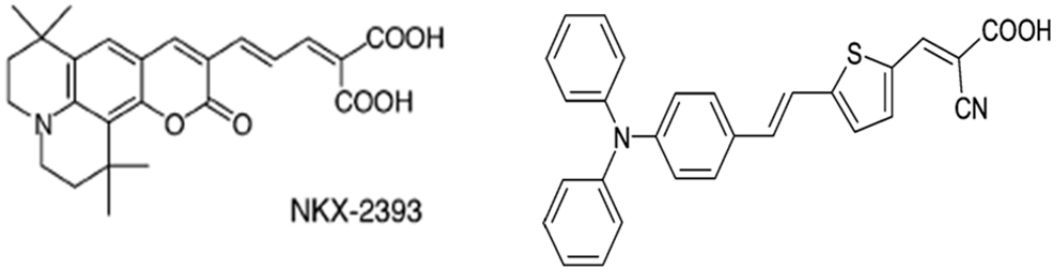

Figure: 3.5 Molecular structure of A- Coumarine. B- Polyene-Diphenylaniline Dye employed as sensitizers in DSSCs

Co-sensitization, the use of two dyes combination that complements each other in their spectral features is another strategy to obtain a broad optical absorption extending throughout the visible and near IR region (138), (139). This strategy has the advantage of enhancing photo-absorption in that the optical effects of the two sensitizers are found to be additive. In particular, there was no negative interference between the co-adsorbed chromophores, opening up the way for testing a multitude of other dye combinations (140). In addition to all these alternatives, fruits, flowers and/or leaves have been employed as sources of natural photosensitizers and reported as cheaper, low-energy and environmentally friendly alternatives for the production of DSSCs (129).

3.2.3.4 The Electrolyte

The electrolyte is an important part of DSSCs. Without it the cell will not work. It acts as the hole-transport material. It is responsible for internal charge carrier between the two electrodes. It regenerates the dye at the working electrode with the charge collected at the counter electrode. When the dye absorbs light it loss electron and becomes oxidized, for stable continues operation of the solar cell, the oxidized dye must be reduced back to its ground state as rapidly as possible by a suitable electron

donor. The electrolyte plays this role and donate electron to the dye. For choosing the electrolyte, it is important for stable performance of the solar cell to consider the following (113);

1- The redox couple must be fully reversible;

2- It should not exhibit significant absorption of light in the visible region

3- Stable in the oxidized and reduced forms.

3.2.3.4.1 Redox couple

So far the best DSSC performance has been obtained using the tri-iodide /iodide (I_3^-/I^-) redox couple in an organic matrix, commonly acetonitrile. The good result of this redox mediator is based on the following kinetics.

1- First, the photo-oxidized dye injects an electron into the conduction band of the semiconductor much faster than electron recombination with I_3^-.

2- Secondly, the oxidized dye preferably reacts with I- than recombines with the injected electron.

3- Finally, the two electron process of I^- [1] regeneration from I_3^- occurs quickly enough at the catalyst-coated counter electrode to be productive.

The overall result of the above processes leads to coherent diffusion of I_3^- towards the counter electrode and I^- diffusion in the opposite direction.

$$2e^- + I_3^- \longleftrightarrow 3I^-$$

Illustration: 3.1 Tri-iodide/iodide redox couple.

When employing this redox couple as electrolyte however, its concentration has to be taken into consideration. Obviously, at low electrolyte concentrations conductivity will be inadequate and rapid reduction will not be ensured. On the other hand, when employing high electrolyte concentrations,

iodide can substantially suppress cell efficiency by increasing the recombination of I_3^- and injected electrons, and increasing the rate of light absorption by the redox couple. The suppression of the dark current (see section 3.2.4.1) may be achieved by additives such as tetrabutylammonium hydroxide (TBAOH) (141) and/or methylbenzimidazole (142). It has also found that, these additives have enhanced the cell's long-term stability (142).

Some other redox couples have also been tested, such as phenothiazine (143), (SeCN)2/SeCN- (144), (SCN)2/SCN- (144) and/or Br3-/Br- (145) and theoretically a well designed change in the electrolyte formulation could increase the Voc by up to 300 mV (146). However, probably the most experienced and most feasible alternative to date is the use of cobalt complexes. Several complexes of Co(II)/Co(III) have been tested (147), (148). Compared to iodide, their advantage is that they are non-volatile, non-corrosive and have the benefit of being easy for molecular modifications. However, with present technology the current exchange rate at the counter electrode is much smaller and leads to voltage losses (148).

3.2.3.4.2 Organic solvent

Regarding the best solvents for the redox couple, hundreds of chemical compounds can be used as long as they fulfill most of the following requirements:

1- Low volatility at the expected cell operating temperature;

2- Low viscosity to easily penetrate the pours semiconductor

3- Resistance to decomposition over long periods of time;

4- Good redox couple stability;

5- Low toxicity and low cost.

Several organic solvents such as methoxypropionitrile (149), butyronitrile (150) and/or methoxyacetonitrile (151) have been tested among others; however, acetonitrile is the most used solvent, particularly when one wishes to maximize cell efficiency.

Even though 11 % conversion efficiency for DSSCs with liquid electrolytes has been achieved, the potential problems caused by liquid electrolytes, such as leakage and volatilization of organic solvents, are considered as some of the critical factors limiting the long-term performance and practical use of DSSCs. A worth mentioning area of research in DSSC regarding electrolytes is the use of room temperature ionic liquids, quasi-solid state and solid state. These electrolytes are progressively viscous enabling increased stability. They appear to solve problems such as dye desorption, solvent evaporation and sealing degradation, however, until now their performance has been consistently lower.

An ideal ionic liquids for DSSC should have good chemical and thermal stability, negligible vapor pressure, non-flammability, high ionic conductivity and a wide electrochemical window (152). Molten salts based on imidazolium iodides have revealed very attractive stability features (153) and (152). Despite their high viscosity, linear photocurrent response up to full solar light intensities has been observed. The best results have been obtained with 1,3-dialkylimidazolium iodide compounds (154).

Solid-state electrolytes overcome the disadvantage of fluidity and volatility for liquid electrolytes, however, poor interface contact property and lower conductivity for solid-state electrolytes lead to lower light-to-electricity conversion efficiency for DSSCs. Quasi-solid-state electrolytes, on the other hand, own comparable liquid electrolyte's ionic conductivity and interface contact property and solid-state electrolyte's long-term stability, it is believed to be one kind of the most available electrolytes for fabricating high photoelectric performance and long-term stability of DSSCs in practical applications.

3.2.4 Technical consideration

3.2.4.1 Dark current

An important point that has to be taken into consideration when trying to get the maximum obtainable cell voltage: is what known as the dark current. The TiO_2 layer is an inter-connected network of particles with high porous interior. The dye should penetrate everywhere and adsorb over a large surface area. The redox mediator must also penetrate the same domain so as to be present in the direct surrounding area of the photo-sensitizer. If the redox mediator reaches to the back contact, dark currents arise from the reduction of the redox mediator by the collector electrode with the oxide layer. Technically, this charge recombination can also occur at surfaces other than that of TiO_2. Due to the spongy nature of the TiO_2 film, it can also happen at the back conducting glass electrode. Dark currents can be suppressed by co-adsorption of saturated hydrocarbons with anchoring groups that isolate the uncovered oxide surfaces from interactions with oxidized form of the redox couple, for example chenodeoxycholic acid (113), (155). Alternatively, introduction of the dye-coated electrode to a solution of a pyridine derivative such as 4-t-butylpyridine has also been found to improve dramatically the efficiency of the cell (113). Another strategy, as mentioned above in this chapter, is to use a compact (117) or nanocrystalline (118), TiO_2 "blocking layer".

3.2.4.2 Dye density on the semiconductor

Sensitization of semiconductor in DSSC is usually done by immersion of the working electrode in a solution of known dye concentration. The dye coverage is controlled by two factors time of immersion and dye concentration. The amount of sensitizer dyes on nano-crystalline semiconductor films is a factor of considerable importance for controlling the performance of DSSCs because performance reduction for highly loaded films has frequently been reported (156), (157), (158). To clarify the origin of the lowered performance, transient absorption (TA) spectroscopy measurements were examined as a function of dye concentration. Hirata found that electron injection efficiency

decreases with increasing concentration of dye on the surface. They explained that this is due to multi-layer adsorption of dyes on the surface (159). Moser and co-workers reported that the electron injection rate was reduced by the aggregation of N3/TiO_2 films by comparing them with N719/TiO_2 films, (160). More recently, Pellnor et al. carefully studied the difference in electron injection dynamics between N3/TiO_2 and N719/TiO_2 by varying experimental conditions such as the observed wavelength and the density of dye on the surface (161). Although they pointed out that the injection dynamics difference between N3/TiO_2 and N719/TiO_2 was mainly due to the difference in temporal spectral change, they observed that the injection dynamics were affected by the density of dye on the surface for N3/TiO_2 films. Hence, more careful considerations are needed to obtain the necessarily amount of dye coverage that give the best cell performance with the amount of dye coverage.

3.2.4.3 Characteristic parameters of DSSCs

3.2.4.3.1 Open circuit voltage

The DS solar cell can be regarded as a battery in a simple electric circuit. In the dark, the cell does nothing. At that point the system is at equilibrium, the Fermi energy of the TiO_2 electrode (corresponding to the free energy of electrons in this film after thermalization) equilibrates with the midpoint potential of the redox couple, resulting in zero output voltage. Under these conditions, the TiO_2 Fermi level lies deep within the band gap of the semiconductor, and the film is effectively insulating, with a negligible electron density in the TiO_2 conduction band. Likewise at the counter electrode, there will be high concentrations of oxidized and reduced redox couple present in the electrolyte and no significant change in chemical potential of the electrolyte, which remains effectively fixed at its resting value. When light hits the working electrode, photo-excitation of the dye injects electron into the TiO_2 film which leads into dramatic increase in electron density, raising the TiO_2 Fermi level towards the conduction band edge, and allowing the film to become conducting. This happen in parallel with hole injection into the redox electrolyte (162). That causes the circuit to switch on and develops a voltage, or

electromotive force (e.m.f.), analogous to the e.m.f. of the battery. Since this developed voltage has occurred when the terminals are isolated (infinite load resistance "shunt resistance") is called the open circuit voltage (Voc) (163) .The magnitude of open-circuit photo-voltage developed is determined by the energy difference between the Fermi level of the solid under illumination and the Nernst potential of the redox couple in the electrolyte (162). However, the experimentally observed open-circuit potential for various sensitizers is smaller than the difference between the conduction band edge and the redox couple, probably due to the competition between electron transfer and charge recombination pathways. Knowledge of the rates and mechanisms of these competing reactions are vital for the design of efficient sensitizers and, thereby, improvement of the solar devices (113).

3.2.4.3.2 Short circuit current

The given current when the terminals are connected together under illumination is called the short circuit current I_{sc}, and is dependent on the incident light. The generated photocurrent is roughly proportional to the illuminated area, for that reason the short circuit current density, J_{sc}, is the useful quantity for comparison (163). In order to relate the photocurrent density, J_{sc}, to the incident spectrum, we need to calculate the Incident Photon to Current Efficiency (IPCE), that shows the probability that an incident photon of energy E will deliver one electron to the external circuit. It can be calculated in the following equation:

$$\text{IPCE} = \frac{(1.25 \times 10^3) \times \text{photocurrent density } (\text{mA cm}^{-2})}{(\text{wavelength } (\text{nm})) \times (\text{photon flux } (\text{Wm}^{-2}))} \qquad \text{Eq. 3.1}$$

For any intermediate load resistance RL, the cell develops a voltage V between 0 and Voc and delivers a current I such that V = I × RL, and I(V) is determined by the current-voltage characteristics of the cell under that illumination, as described above. However, when a load is present, a potential difference develops between the terminals of the cell, and this potential difference generates a current

which acts in the opposite direction to the photocurrent, and the net current is reduced from its short circuit value. This reverse current is usually called the **dark current** in analogy with the current which flows across the device under an applied voltage V in the dark.

Most solar cells behave like a diode in the dark, admitting a much larger current under forward bias (V > 0) than under reverse bias (V < 0). This rectifying behavior is a feature of photovoltaic devices, since an asymmetric junction is needed to achieve charge separation. The overall current voltage response of the cell, its current-voltage characteristics, can be approximated as the sum of the short circuit photocurrent and the dark current (163).

The cell power density is given by the equation: $P = J \times V$ Eq. 3.2

The power density of the cell reaches a maximum power point, which occurs at some voltage V_p with a corresponding current density J_p, as shown in figure 3.4.

3.2.4.3.3 The fill factor

The fill factor (ff) is defined as the ratio of the maximum power from the solar cell to the product of Voc and Jsc, and describes the "squareness" of the J-V curve. Graphically, the maximum power density or fill factor is given by the area of the rectangle formed by $J_p \times V_p$ (see figure 3.4). The outer rectangle has an area $J_{sc} \times V_{oc}$. If the fill factor was equal to 1, the current voltage curve would follow the outer rectangle.

$$FF = \frac{\mathrm{Vmax}}{Voc} \times \frac{\mathrm{Jmax}}{Jsc} \qquad \text{Eq. 3.3}$$

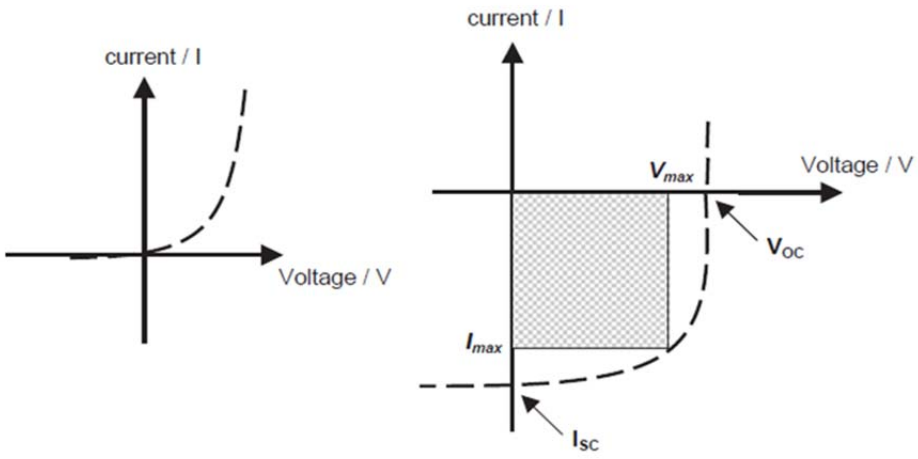

Figure: 3.4 I–V curves of an organic PV cell under dark (left) and illuminated (right) conditions.

3.2.4.3.3The global efficiency

The global efficiency, η global, of the cell is the power density delivered divided by incident light power density, Is, and is related to J_{sc} and V_{oc} using the ff: These four quantities: J_{sc}, V_{oc}, ff and η global are the key parameters for testing the solar cell performance. They should be defined for particular illumination conditions. The Standard Test Condition (STC) for solar cells is the Air Mass (AM) 1.5 spectrum (see chapter one), an incident power density of 1000 $mW \bullet m^{-2}$ (1 sun) and a temperature of 25°C (163).

$$\eta = \frac{\mathrm{Voc} \times \mathrm{Jsc} \times FF}{Pin} \qquad \text{Eq. 3.4}$$

Chapter: 4 Material and methods

4.1 ASPHALTENE PREPARATION

Petroleum asphaltene are defined as the n-pentane or n-heptane insoluble but toluene soluble / fraction of crude oils. This operational definition is a consequence of the extremely complex structure of asphaltene which consist of thousands of compounds containing highly aromatic cores, long chain aliphatic groups, heteroatoms (sulfur, nitrogen, and oxygen) as well as trace quantities of heavy metals (vanadium and nickel, iron, etc). Therefore, it is extremely difficult to get a definite molecular structure, for this reason we tried to fractionate it into some sub-fraction according to their solubility class and use them as light harvesting material in DSSC.

4.1.1 Extraction of asphaltene

For the first trail asphaltene dye sentsized solar cells presented in this dissertation, the used asphaltene was either obtained from the upgrading experiment or extracted by using hexane as solvent, it will be referred to as hexane asphaltene or by the associated experimental number. The crude oil used was Canadian Tar sands for the first trials or latter on Altamira Hunt Crude oil. As the project proceeds, the asphaltene were extracted from the crudes as follows: The crude oil sample was separated into maltenes (n-heptanes soluble) and asphaltene (n-heptene insoluble) by adding n-heptanes in a volume-volume ratio of n-heptanes to crude oil of 40: 1 followed by filtration. A 50 ml of crude was mixed with 2000 ml of n-heptane in a beaker, the mixture then stirred by magnetic tip overnight at room temperature. The used solvent-to-oil ratio of 40:1 has been demonstrated to be suitable for avoiding errors in the determination of the amount of asphaltene fraction and in its characterization (164). The mixture was filtered using a filter paper No 40 with a pore diameter of 8 μm. The obtained asphaltene contains parts of oil that does not dissolve in heptanes such as clay, sand etc. for this reason it was purified by dissolving it completely in toluene at room temperature and then filtered again to remove debris. The obtained solution of asphaltene and toluene was covered and kept under vacuum at room

temperature for 24 hours to dry out. The precipitated asphaltene then weighted for determining asphaltene content, marked as crude asphaltene and will be referred to as un- fractionated asphaltene throughout this dissertation.

Table: 4.1 Yields of asphaltene extracted from 50 ml crude oil

Asphaltene	Unpurified	Purified	Impurities
Wt. gram	6.46	6.27	0.19

4.1.2 Fractionation of asphaltene

A sample of 3 g asphaltene was dissolved in 100 mL toluene, and 300 mL n-pentane was added into the solution and mixing by stirring with a magnetic bar at ambient temperature. After adding n-pentane, the ratio of the total volume of the n-pentane to toluene is kept at 75/25 in volume. The solution was covered and stirred for half an hour for precipitation of insoluble. After filtration, the insoluble fraction was collected and dried at room temperature and left under vacuum overnight to obtain the first fraction (First precipitate. Fr.1). another amount of 270 ml pentane then added to the filtrate n-pentane and toluene to keep the ratio of the total volume of the n-pentane to toluene at 85/15 in volume.

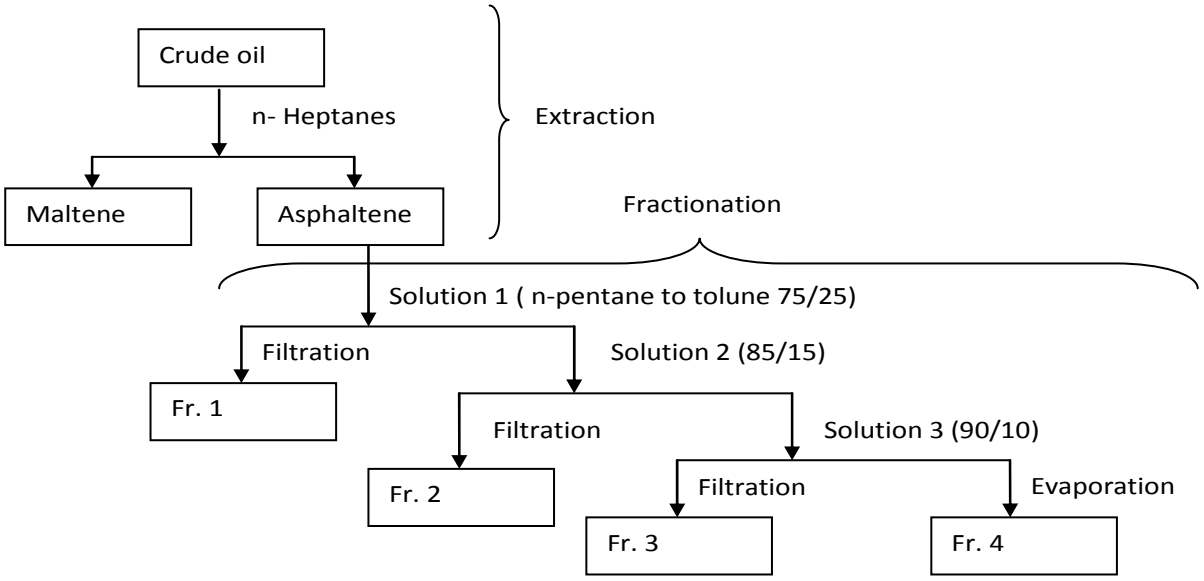

Illustration: 4.1 Asphaltene extraction and fractionation procedure

The filtration and drying process then repeated following the procedure described above, (Second precipitate. Fr. 2) was precipitated in a solution with an n-pentane to toluene ratio of 85/15 in volume. Similarly, samples (Third precipitate. Fr.3) (n-pentane to toluene = 90/10), were precipitated in binary solutions with the increasing proportion of n-pentane. The last fraction, (fourth precipitate Fr. 4), was obtained by evaporating the solvents with the remaining asphaltene. The asphaltene extraction and fractionation scheme is shown in Figure 4.1.

Table: 4.2 Yields of solvent sub-fractions of 3 gram asphaltene

Sub-fraction	Fr. 1	Fr.2	Fr.3	Fr.4	Loss
Wt. gram	0.12	0.63	0.07	1.10	1.08

4.1.3 Asphaltene thin films

To measure the absorption spectra of asphaltene, a thin film of different asphaltene fraction has been deposited onto clean glass substrate by using spin coating technique. Absorption spectra of this thin film have been recorded using UV.VIS spectrophotometer. In the procedures; 0.002 gram of every asphaltene fraction was added to 20 ml toluene and dissolved completely by the aid of sonic machine. The substrate was placed on the spin coater chamber, and an appropriate amount of asphaltene solution was applied on the surface of the glass substrate using syringe and needle. The spin coating speed was kept at 2500 rpm. The coating was done on plain glass slides which were not transmittance to UV so the UV spectra were eliminated. The time of spin coating was 30 seconds. After spin coating, the films were left in clean plastic box for visible light absorption.

4.2 BUILDING THE DSSC

4.2.1 The used TiO_2 paste

Three TiO_2 pastes were used in this study. The first paste was prepared in our lab according to the procedures published in literature (165). This will be referred to as homemade TiO_2 paste. In the procedure a 6 grams of commercial TiO_2 powder (P25) obtained from Sigma Aldrich Company were mixed with 1 ml of acetic acid and grinded in a mortar for 5 minutes. A total of 5 ml D. water plus 15 ml ethanol were added ml by ml with continue grinding. The amount of added ethanol was then increased to 2.5 for 6 times and grinding for 1 minute for every addition. The paste was then transferred to a beaker with the help of addition of 100 ml ethanol, and stirred with magnetic tip and sonicate with ultrasonic horn for 2 seconds work + 2 second rest for 30 times. A 20 gram of terpineol was added with repeating the sonciation procedure. Finally, 3 gram of ethyl cellulose was added and repeating the above mentioned sonciation procedure. The ethanol then evaporated by the help of a rotary evaporator. A schematic diagram showing the fabrication procedure is shown below.

The other two TiO_2 paste used in this research were a commercial highly transparent Ti-Nanoxide HT/SP and Ti-Nanoxide R/SP obtained from Solaronix Company Switzerland. The first paste contains approximately 18 % wt. of nano-crystalline titanium dioxide with 8-10 nm particle size, with terpineol and other organic binders. A layer of highly porous anatase nanocrystals is obtained after firing at 450 °C for 30 minutes. The obtained sintered layer is highly transparent.

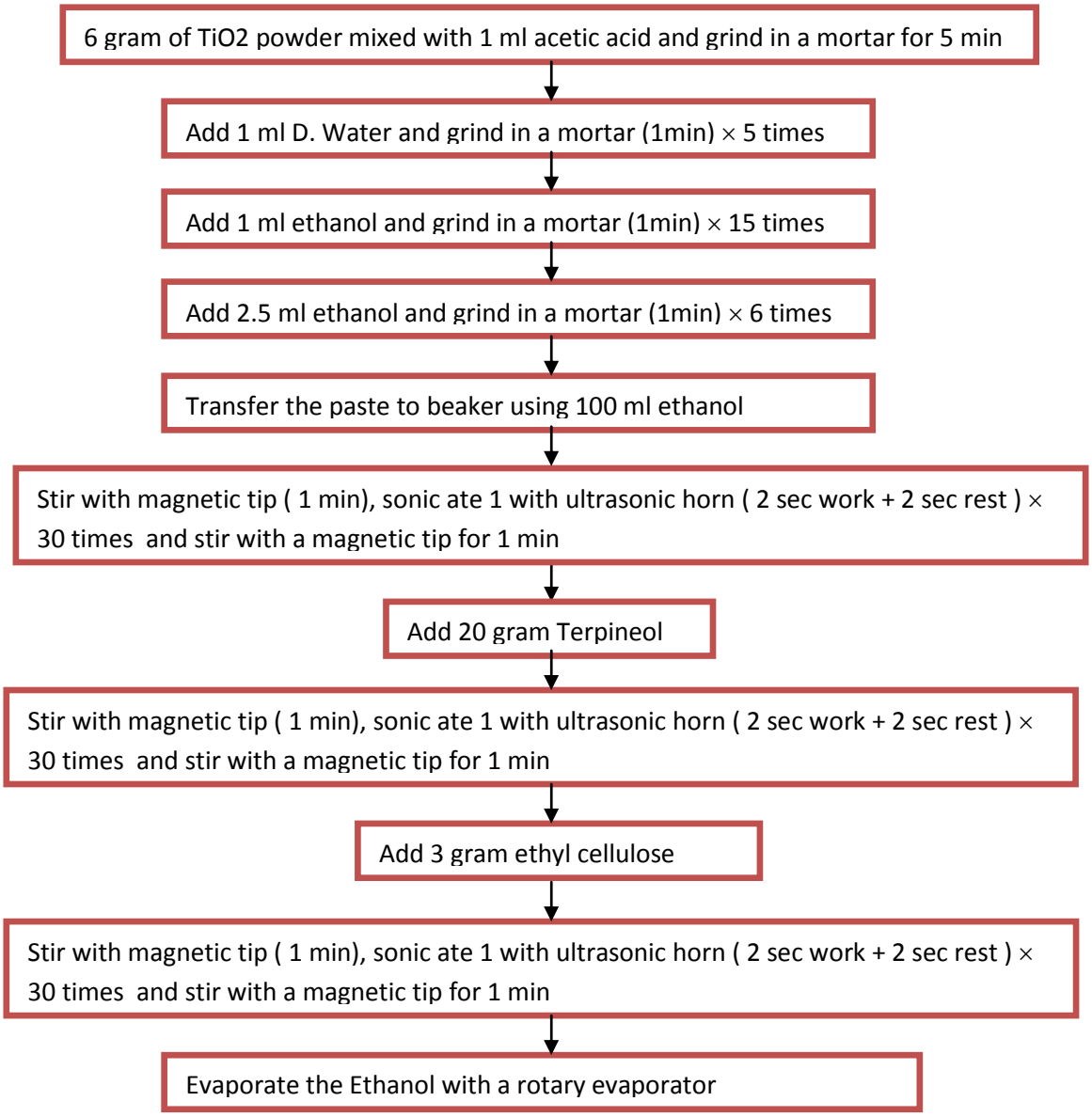

Illustration: 4.2 preparation of the homemade TiO_2 paste

4.2.2 Preparation of the photo-electrode

4.2.2.1 The Blocking layer (compact TiO_2 layer)

The blocking layer was prepared in the following manner. The FTO glass was first cleaned in a detergent solution using an ultrasonic bath for 15 min, and then rinsed with water and ethanol, after that the FTO glass plates were immersed into a 50 mM aqueous solution of $TiCl_4$ at 70 C for 30 min and washed with water and ethanol. The $TiCl_4$ solution was formed by mixing 0.54 ml $Ticl_4$ in 100 ml of ultra water in an ice path.

4.2.2.2 Nanocrystalline TiO2 layer

The nanocrystalline TiO_2 layer in this study was prepared by applying a layer of one or more of the above mentioned TiO_2 pastes by spreading (doctor blading) on a conductive transparent surface of a piece of glass (F-doped SnO_2, FTO, (Sloarnoix TCO30-8 SA Switzerland 8 Ω/cm^2/&,3.3 mm thickness and 500- 1000 nm transmittance) that had been cut to 5 x 2.5 cm and cleaned with D water and ethanol. The FTO-coated glass was covered with two layers of parallel adhesive Scotch tape 1 cm apart to control the area and the thickness of the TiO_2 film (3 x 1 cm) see figure 4.1.

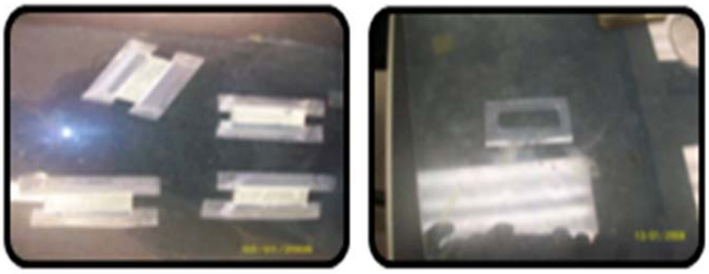

A B

Figure: 4.1 A-Applying the TiO_2 paste B- Photo electrode after asphaltene absorption

The colloidal paste was applied between the tapes on the FTO-coated glass by rolling a glass rod on the surface. The film thickness is controlled by the paste concentration and the adhesive tape thickness as well. Film thickness was in both cases, typically 8 ± 10 μm. The TiO_2 nanocrystalline electrode was dried in air for 20 minutes, and then heated in a tube furnace at 450°C for 30 min with air supply. The heating processes enable the added organic polymer in the colloidal paste to be burnt off leaving the TiO_2 film with higher surface area and more porous. It also increases the resistivity of the film. In addition, the surface is dehydroxylated during this process, leaving reactive Ti_3^+ centers available for reaction with the anchoring groups of the sensitizers. To minimize rehydration of the TiO_2 surface from moisture at ambient air (which causes dye desorption), the electrodes, while still warm (50-70°C) from annealing, were immersed into a solution of asphaltene for several hours depending on the

experiment that was carried out. The porous oxide layer acts like a sponge and there is efficient uptake of the asphaltene, leading to intense coloration of the film.

4.2.3 Preparation of the counter electrode

To prepare the counter electrode, two holes were drilled in the FTO glass (Sloarnoix TCO22-7 a 2.2 mm thick soda-lime glass coated on one side with a fluorine doped tin oxide SnO2:F) layer ("FTO" glass) by diamond coated drill. The sheet resistance of the FTO layer is ~7 ohm/square. The perforated sheet was washed with H_2O as well as with ethanol and cleaned by ultrasound in an ethanol bath for 10 min. After cleaning, the Pt catalyst was deposited on the FTO glass by coating with drops of H_2PtCl_6 solution (2 mg Pt in 1ml ethanol) and repeating the heat treatment at $450^{O}C$ for 15 min. The platinum coating on the counter electrodes acts as catalyst reducing the oxidized form of the electrolyte (see chapter 3.2.3.2.).

4.2.4 The electrolyte

Two type of commercial electrolytes obtained from Solaronix company have been used in this study. They are Standard Iodolyte MPN-100. It consists of 100 mM of tri-iodide in methoxypropionitrile solution. The second one is Iodolyte TG-50. It is Iodide Based Redox Electrolyte consists of 50 mM of tri-iodide in tetraglyme.

4.2.5 Assembling the asphaltene DSSC

The asphaltene covered TiO_2 electrode (cleaned with toluene after taken out of the asphaltene solution) and Pt-counter electrode were assembled into a sandwich type cell and sealed with a two layers of Surlyn thermoplastic hot-melt sealing foil of 60 μm thickness made of the SA SX1170-60 Solaronix. The sealant was used to connect the two electrodes and to provide space for the electrolyte between two electrodes. To get the good sealant the sandwich of electrodes was heated on the heating plate at 100 C^{o} for 10 to 15 sec while pressing them together. A drop of the electrolyte solution was introduced into the hole in the back of the counter electrode and covered the hole with tape. The electrolyte was introduced

into the cell via vacuum backfilling by inserting a needle of a syringe in a piece of rubber that glued into the surface of the counter electrode. The following figure is a sketch of completed asphaltene DSSC.

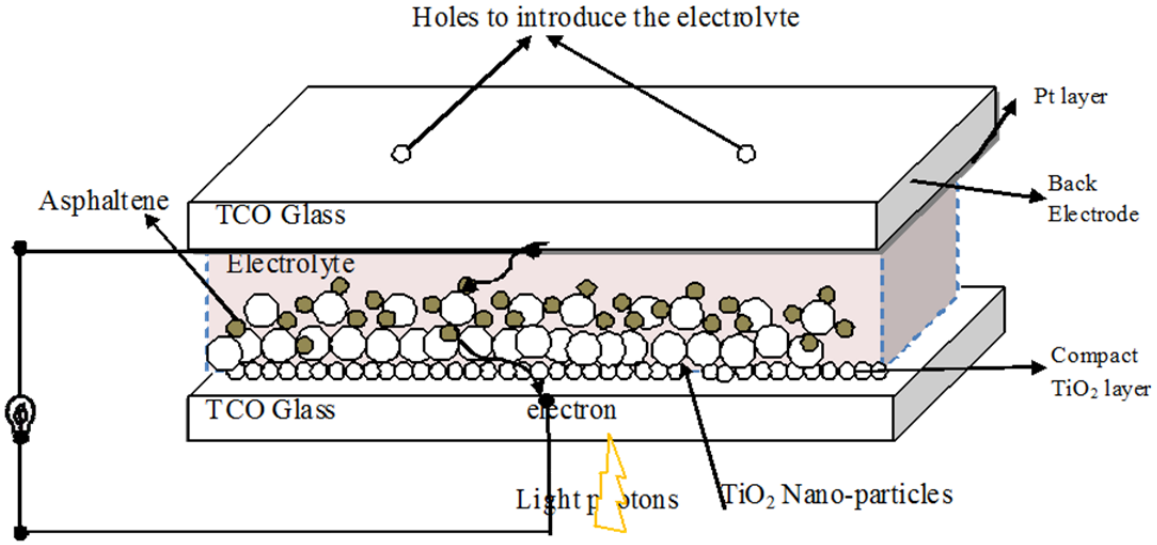

Illustration: 4.3 Schematic diagram showing completed asphaltene DSSC

Chapter: 5 Results and Discussion

5.1 INTRODUCTION

Some of the following experimental results have been included in the provisional form of the United State Patent Application No 20090114283 U.S. Provisional Application Serial No. 61/224, 791132, described as Asphaltene Based Photovoltaic Devices.

5.2 FIRST EMBODIMENT ASPHALTENE SOLAR CELL

Table 2, 3, 4 in the above mentioned patent are the results of our first embodiment asphaltene DSSC that produces current and voltage when shined by light (see table 5.1,5.2).Asphaltene fractionation technique used here was by titration of asphaltene toluene solution with pentane until the precipitate starts appearing. The first precipitate (fr.1) collected at 100 ml pentane addition and the second at 200 ml pentane. The photo-electrode of this cell is composed of one layer of our homemade TiO_2 paste mentioned in (chapter 4.2.1) and no blocking or compact layer were used. The asphaltene was hexane extracted asphaltene, obtained from Canadian Tar Sands. Two solvents (Benzene and Toluene) were utilized to make the asphaltene solution. Toluene gave much better result when applied as solvent to spread the asphaltene over the photo-electrode. Hence, it has been chosen as the preferred solvent in the upcoming asphaltene solar cell presented in this dissertation. The counter electrode was prepared according to the procedure described above (See 4.2.3). Two asphaltene concentration; 0.5 g/l and 0.25 g/l were used. The less asphaltene concentration gave better results see table 5.1, table 5.2. The cells were tested by Multimeter VOM (Volt-Ohm meter), and under direct Sun rays.

Table: 5.1 Current and voltage results of the first 0.5 g/l asphaltene DSSCs

ASPHALTENE	FR.1	FR.2	FR.3	FR. 4	UNFR. TOLUNE	UNFR. BENZENE
Current (μA)	0.2	1.1	1.5	2	0.1	0.01
Voltage (mV)	11.7	1.2	1.6	5.7	7.02	2.3

Table: 5.2 Current and voltage results of the first 0.25 g/l asphaltene DSSCs

ASPHALTENE	FR.2	FR. 4	FR.4*	FR.3#	FR.3*#
Current (μA)	12	4.1	7	23	40
Voltage (mV)	14	4.1	6.8	52	273

The performance of FR. 3 cell with two layers of TiO_2 paste increased on the second day and then declined sharply. After a visual inspection of the cell it was discovered that, some colored spots start appearing on the back electrode as indication of the electrolyte touching the counter electrode, which was not in on the second day. This causes electrons produced from the excited asphaltene to recombine with ions in the electrolyte and thus reduces the current of the cell. The explanation of increasing the cell performance on the second day is probably due to the saturation of pores in the paste with electrolyte which takes time as it happens by the capillary action (see chapter 4.4.2). Testing the cell under solar simulator shows a diode characteristic curve, see figure (5.1).

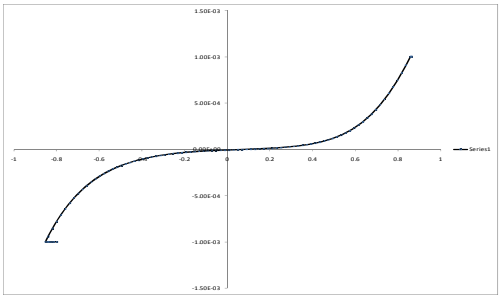

Figure: 5.1 Diode curve of the first embodiment asphaltene solar cell.

* Measurements after one day

Two TiO_2 layers

From this set of results, one can withdraw the following conclusions:

1- Asphaltene could be a good photo-sentsizer.

2- There are some differences in cell output with asphaltene fraction and concentration.

3- The thickness of TiO_2 layer has a great impact on cell performance

4- Leaving the cell for one day produces better results.

5- Toluene gave much better result when applied as solvent to spread the asphaltene over the photo-electrode.

6- It was also observed that TiO_2 paste peel off from the FTO glass surface.

5.2 IMPROVING THE PERFORMANCE OF ASPHALTENE DSSC

After our first cell showed a characteristic diode curve which was an indication of photovoltaic effect, we start working on enhancing the performance of these cells by improving the manufacturing processes and materials. Our purpose was first to perfect the manufacturing processes of the cell and obtain reproducible cells with fewer errors, then to vary the asphaltene variables. Taking into account the above mentioned comments, we have done the following; increased the thickness of the TiO_2 layer to two layers; leave the cells overnight before testing; use toluene as solvent to spread the asphaltene over the photo-electrode; and incorporating the compact layer to adhere the TiO_2 paste on the FTO glass.

5.2.1 Introducing TiO_2 compact Layer

The importance of a blocking layer in organic dye-sensitized solar cells has been demonstrated in many studies (166), (167), (168), (169). It was shown that upon the addition of a compact layer, the light-harvesting efficiencies were more than tripled. Such a compact layer improves the adhesion of the TiO_2 to the TCO and provides a larger TiO_2/TCO contact area and more effective electron transfer from

theTiO_2 to the TCO by preventing the electron recombination process (see 3.2.4.1), which occurs in the interface between the redox electrolyte and the TCO surface. The compact layer can be fabricated by various methods such as sputter deposition (166), dip-coating (167), chemical vapor deposition (168), and spray pyrolysis (169). Especially, the fabrication of theTiO_2 compact layer using a $TiCl_4$ aqueous solution has been widely adopted (166) and is the method used in this research.

To test the effect of the compact TiO_2 layer on the performance of asphaltene solar cells we made two asphaltene solar cells both with three TiO_2 layers (one compact and the other is Nano-crystaline layer). The used paste in these cells was commercial highly transparent Ti-Nanoxide HT/SP paste stated above, and the TiO_2 compact layer was prepared using $TiCl_4$ aqueous solution see (4.2.2.1). The asphaltene was un-fractionated unpurified Hunt asphaltene obtained from Altimera crude oil with utilized concentration of 0.5 g/l.

Table: 5.3 The effect of TiO_2 compact layer on asphaltene cell performance

Cell id	Voc (v)	Jsc (mA/cm^2)	FF %	IPCE %	Voc Slope (ohms)
With compact	0.4784	0.158	35.42	0.03	1830
With compact	0.420	0.388	46.46	0.07	398

The cells were tested under a solar simulator at standard condition of 1.5 sun and the results are shown in table 5.1. It is clear that, the introduction of TiO_2 compact layer prepared by the above mentioned method has increased the short circuit current, the fill factor as well as overall cell efficiency.

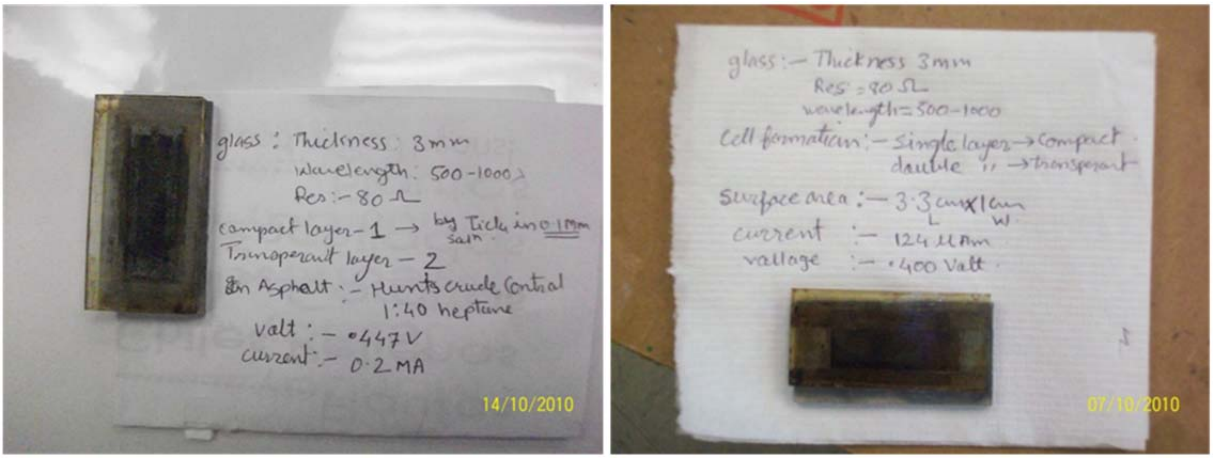

Figure: 5.2 Asphaltene DSSCs with one compact layer

5.2.2 Improving the fill factor by decreasing series resistance

From the above table, even though the two cells were manufactured by the same procedures with one compact layer and two transparent TiO_2 layer there was a big difference in their performance. This difference was clear as a result of their series resistance. Accordingly, in order to better improve asphaltene DSSCs more work should be done on minimizing series resistance.

5.2.2.1 Purifying asphaltene and using RTV silicone rubber mask layer on the photoelectrode

Figure: 5.3 Purifying asphaltene and using RTV mask layer.

A typical DSSC usually contains three interfaces formed by FTO/TiO_2, TiO_2/dye/electrolyte, and electrolyte/Pt-FTO. Simultaneously, electrons are transferred to tri-iodide at the TiO_2/dye/electrolyte interface and iodide is reduced to triiodide at the counter electrode. Series resistance in DSSC could

arise from one of the above interfaces and have a great impact on cell performance. The values of series resistance can be raised by varying the electrical properties of TCO, increasing the thickness of the electrolyte layer and the catalytic activity of the counter electrode. Many researchers (170), (171) (172) have found that, under short circuit conditions, electron transport was predominately affected by the series resistance in TCO-dye interface, and the electrolyte/Pt-TCO interface.

The extraction of asphaltene from crude oil involves dissolving the crude oil in *n*-heptanes followed by filtration. Asphaltene is the part of crude oil that does not dissolve and stay on top of the filter paper. Asphaltene extracted by this method could contain inorganic impurities which may increase resistivity of the asphaltene films when applied on top of TiO_2. Hence, it may have an effect on charge transfer and increases the series resistance at TiO_2/asphaltene/electrolyte interface. For this purpose we employed the purification method described above (chapter 4.2.1) to take off these impurities, before using it in DSSC.

In addition to that, when applying the compact layer in our previous experiments, the FTO glass was immersed completely in a $TiCl_4$ aqueous solution. Subsequently, TiO_2 compact layer was formed on all the TCO coating of the FTO glass used to prepare the photoelctrode. This has shown to increase the resistivity of the TCO layer, for that reason we used RTV silicone rubber paste as mask and cover the backside of glass completely and leave less than half side of conducting surface uncovered, which will be used to deposit the paste. Following these two strategies the efficiency of our cells has increased significantly when compared to previous cells from 0.07 see table 5.1 above to 0.25 see table 5.2 below.

Table: 5.4 Purified Un-fractionated Hunt asphaltene cell parameters with 0.5 gm/ l

Iv parameter	80 mW/cm^2	100 mW/cm^2	120 mW/cm^2	Dark
Voc (V)	0.54	0.55	0.54	0.26
Jsc (mA/cm^2)	0.59	0.72	0.91	0.013
Fill factor %	65.4	63.2	60.6	NA
Voc slope (ohms)	43.6	42.6	38.7	NA
Efficiency (%)	0.26	0.25	0.25	NA

It is clear that the enhancement of cell efficiency in this cell was a consequence of decreasing series resistance and increasing close circuit current which leads to increase fill factor. This is in agreement of other people findings, who found an increase of FF with decrease in series resistance (173) . To study the effect of varying light intensity on cell performance, the cell was tested under three different intensity levels 80, 100, and 120 mW/cm^2. As was expected higher light intensity produces higher current density but less fill factor and therefore lower cell efficiency. This observation is a well known phenomena in DSS cells (174). This is probably due to increase recommendation processes. The existence of the recombination process can be verified in the dark current measurement column five in the above table.

5.2.2.2 Varying asphaltene concentration

To see if the asphaltene concentration has an effect on the performance of asphaltene DSSC, we have made three different solar cells with three different asphaltene solutions (0.5 g/l, 1g/l and 10 g/l). Our initial plan was to use 0.5, 1, 2 g/l but because of human mistake of measuring the concentration, we used 10 g/l instead of 2g/l. To prepare the asphaltene solution we used 0.02, 0.005, and 0.001 grams unfractionated purified asphaltene dissolved in 20 ml toluene. We followed the same procedures described above in 5.2.2.1 and chapter 4 for preparing both the electrodes as well as building the cell. The results are shown below.

Table: 5.5The effect of asphaltene concentration on DSSC performance at 80 mW/ cm^2

Asphaltene Con. / cell parameter	10 g/l	0.5 g/l	1 g/L
Voc (V)	0.58	0.54	0.57
Jsc (mA/cm^2)	0.3	0.59	0.85
Fill factor (%)	43.5	65.36	52.26
Voc slope (ohms)	248	43.6	50.0
Efficiency (%)	0.1	0.26	0.31
Dark current	0.013	0.02	0.019

From the above table it is evident that asphaltene concentration has a great impact on series resistance, current density and fill factor. While there was no significant change in open circuit voltage, at high asphaltene concentration of 10 g/l both the current density, and fill factor decreased sharply which was coupled with increased series resistance.

The explanation of this decrease is probably due to asphaltene aggregation. This phenomena is well documented in the literature of asphaltene see (ch.2) and in agreement with using Porphyrin Sensitizers (one molecular that is shown to occur in the asphaltenic part of crude oil in DSSC (175). Aggregates decreased the photocurrent generation in devices made of tetrachelate porphyrin chromophores, and some push-pull porphyrins suffer from dye aggregation as well (176). The strategy to suppress dye aggregation on the TiO_2 surface is to add a co-adsorbate into the dye solution when fabricating sensitized TiO_2 films into devices. The lower current density and cell efficiency in 0.5 asphaltene cell when compared to 1g/l one is an indication of lower asphaltene absorption on the TiO_2 layer. The fill factor effect can be better viewed by plotting the open circuit voltage and current density of the above cells, see figures 5.3, 5.4 and 5.5. It is obvious that 0.5 asphaltene cell produced the best squared curve of the J-V curve (figure 5.4) which corresponds to the best fill factor table 5.5. However, this cell has the lowest efficiency. Since the photoelctrodes of all these three cells were left in the

asphaltene solution for the same time, this could introduce another variable that could improve cell performance (immersion time).

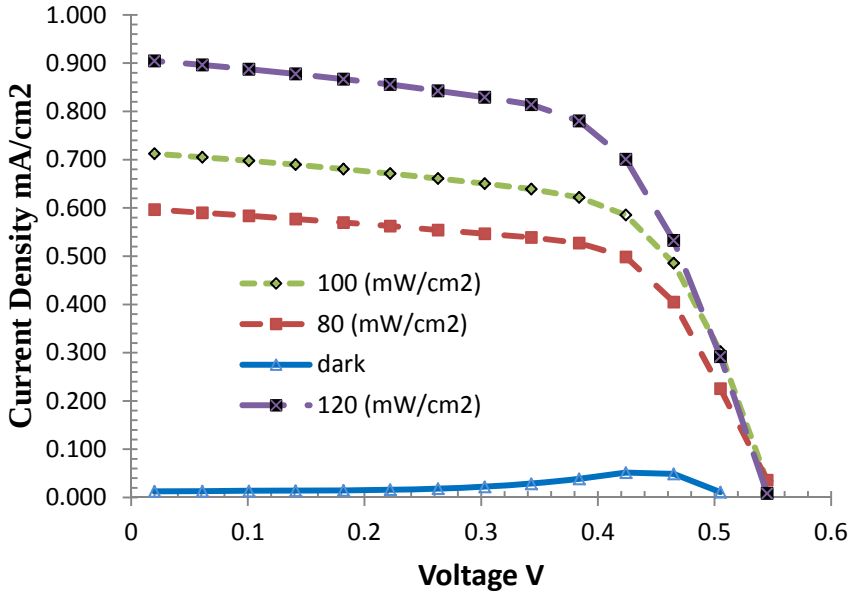

Figure: 5.4 Plot of current density Vs Open circuit voltage of 0.5 asphaltene cell at varied illumination levels

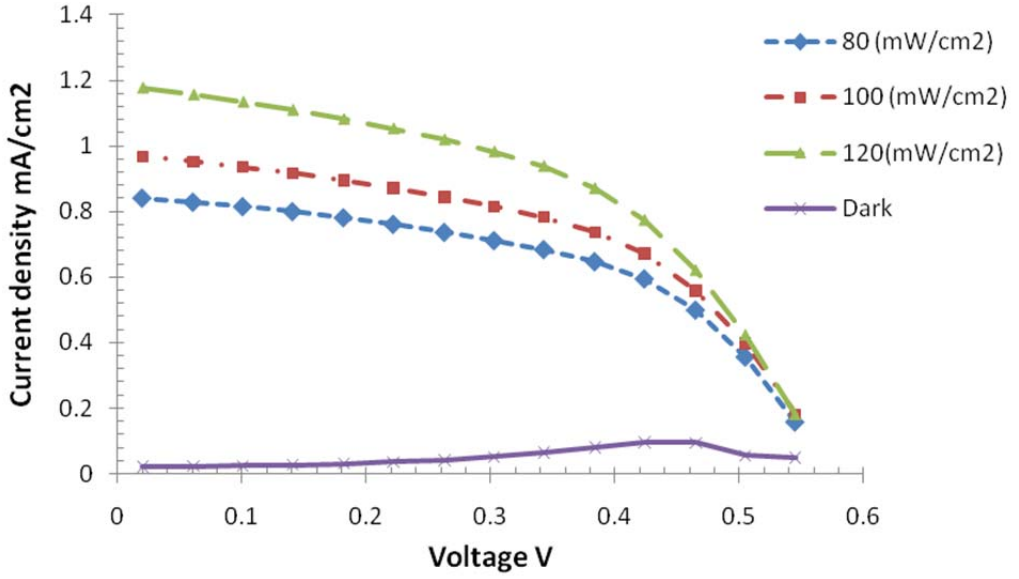

Figure: 5.5 Plot of current density Vs Open circuit voltage of 1g asphaltene cell at varied illumination levels

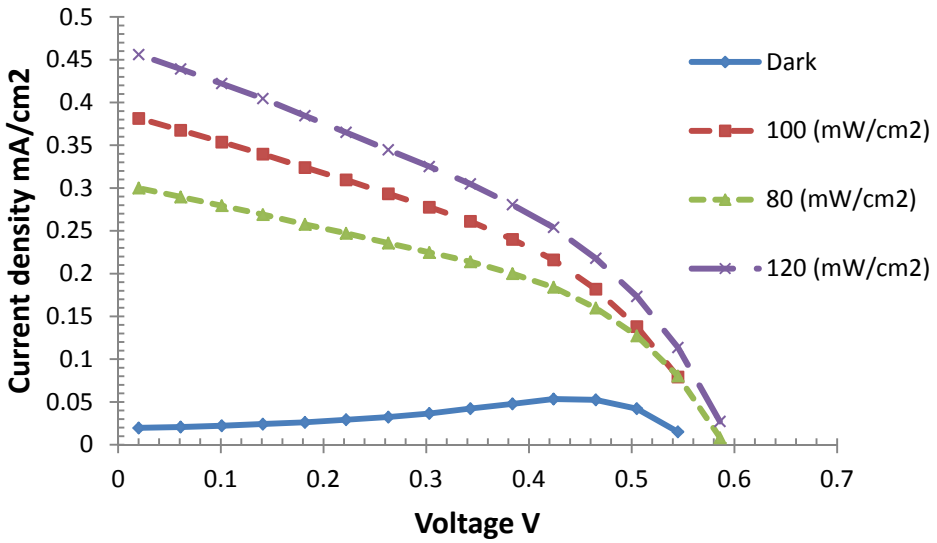

Figure: 5.6 Plot of current density Vs open circuit voltage of 10 g asphaltene cell at varied illumination levels

The variation of dark current in all above cells could be a result of imperfect sealing of the cells, since it was done on hot plate and not using hot press where one can control temperature, time as well as the applied pressure. The used sealant here was Surlyn thermoplastic hot-melt sealing foil of 60 µm thickness purchased from Solaronix.

5.2.3 Increasing the short circuit current and open circuit voltage

The overall efficiency of any solar cell (see chapter 3.2.4.3.3) is the product of fill factor (FF), open circuit voltage and short circuit current. The improvement in the last asphaltene solar cell was a consequence of increasing the fill factor by decreasing the series resistance with concurrent small improvement in both open circuit voltage and short circuit current. In order to make asphaltene competitive to other dyes used in DSSC we need to increase both open circuit voltage and short circuit current.

5.2.3.1 UV-Ozone treatment of the photo-electrode

The main components of the TiO_2 pastes utilized in this study as well as in most DSSC research labs more than TiO_2 particles are organic compounds used to disperse and link the semiconductor particles to form a network film. At high temperature sintering processes these compounds decompose and permit the formation of porous TiO_2 films with high surface area. However, some carbon atoms will probably deposit on top of TiO_2 particles and hinder the absorption of the dye, and the electron injection. UV–O3 treatment is well known method to remove organics on transparent conducting oxides and has been widely used in organic electronic devices to clean the surface and modify the work function of ITO. Recently UV–O3 treatment was applied to synthesize porous nano-particulateTiO_2 films at room temperature and remarkable improvement of photo-conversion efficiency was obtained using the treatment. It is believed that the main effect of the UV–O3 treatment was reported to be the removal of residual organics and positive shift in the conduction band of the nano-crystalline titanium dioxide, which promotes electron injection from the dye (177) (178).

To see if UV–O3 treatment has an effect on the performance of asphaltene solar cells, UV–O3 treatment was first applied on the last TiO_2 layer. Two asphaltene cells were made this time one with the commercial paste and the other is homemade paste described above (4.2.1). Both cells have given much better Voc and photocurrent when compared to the previous cells without UV-O treatments see table 5.6

Table: 5.6 the effect of UV-O treatment on top TiO_2 layer

Cell id	Voc (V)	Jsc m A/cm^2	FF %	IPCE %
Ti HT/SP + R	0.806	8.51	15	1.03
H P25 + R	0.809	6.77	14.7	0.8

After, our UV–O3 treatment on top layer of the photo-electrode showed improvement in cell operation, we apply UV-O3 in three processing steps; on bare FTO before the compact layer, before and

after the compact layer and after the mesolayer. The used asphaltene here was fr.2 asphaltene with applying concentration of 1mg/ml. Due to difficulty of applying the previous sealing material, the sealant has changed to Polypropylene w/ Rubber Medium Adhesive tape with 228.6 micrometers thick obtained from Grainger company item no 6JT54, the adhesive was not strong enough so some drops of crazy glue was put in on top of the tape between the electrodes. So the thickness was further increased a few micrometers. The results are shown in table 5.7.

The efficiency of these cells has increased four times when compared with the ones without UV–O3 treatment. The improvement in efficiency was a result of a big boost in both short circuit current and open circuit voltage. This enhancement was a result of increase in asphaltene absorption, eliminating organic contamination and therefore, higher photon capture and higher electron injection. However these cells shows very low fill factor. The decrease in the fill factor is due to increasing the electrolyte thickness as a result of increasing the sealant layer. The electrolyte ions will take longer time to reach the counter electrode before it reduced back. Similar results were observed with increasing the electrolyte thickness see 5.2.2.1.

Table: 5.7 The effect of ozone treatment on the asphaltene DSSC

IPCE (%)	Voc (V)	Jsc (mA/cm^2)	FF (%)	FTO UVO	CL UVO	ML UVO
1.44	0.8252	13.19	13.1	X		X
1.34	0.7818	13.55	12.9	X	X	
0.76	0.7790	7.74	12.2	X	X	X

The low photo current in asphaltene solar cell when UVO treatment was done on all the three TiO_2 layers was probably due to electrolyte touching the counter electrode because of improper sealing. So changing the sealant is vital at this point.

5.2.3.1 Varying asphaltene fraction

The open circuit voltage and short circuit current are both depend on the extent of light absorption. The most straightforward way to increase Jsc is to absorb a greater fraction of the incident light. The optical gap of the Ru dye in the most efficient DSSC to date is 1.8 eV, allowing it to absorb essentially all the light out to 700 nm. Increasing the photocurrent density requires decreasing the optical gap to extend the dye's absorption into the near-infrared. Our first thought of increasing short circuit current is to try different asphaltene fraction. Fractionation of asphaltene produces slightly different absorption spectra (see figure 5.6)

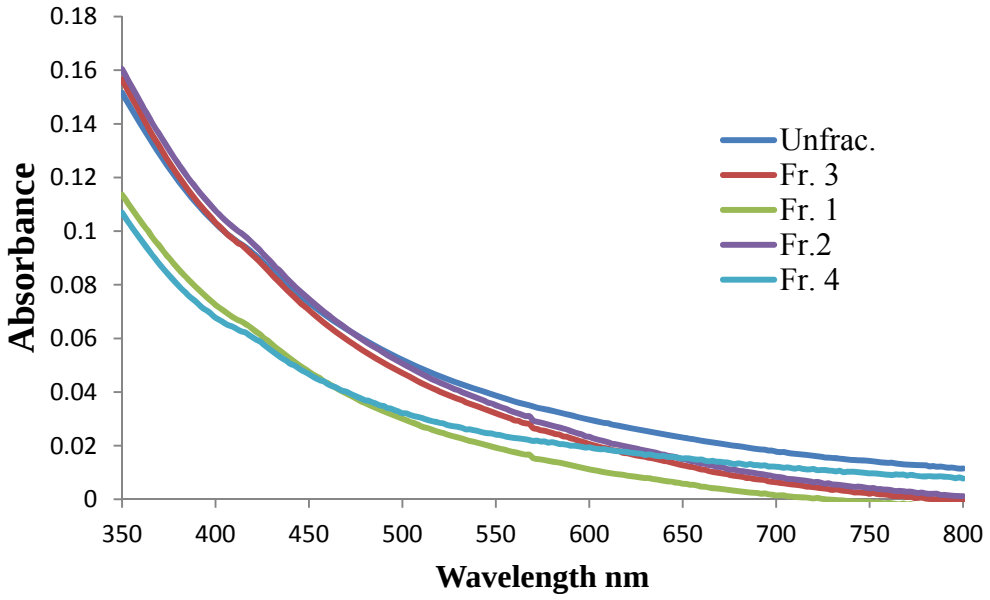

Figure: 5.7 Absorption spectra of asphaltene thin films

Neglecting the fill factor at the moment, the cells made of Fraction four which is the most toluene soluble fraction produces the less photocurrent and photo voltage when compared to the other asphaltene fractions. The less soluble asphaltene part (fraction one) generates higher photo voltage but lower photocurrent then fr.2, (see table 5.5) fr.3, and un-fractionated asphaltene.

Table: 5.7 Asphaltene fraction cell parameters

IPCE (%)	Voc (V)	Jsc (mA/cm^2)	FF (%)	Frac #
1.80	0.7793	13.69	16.6	3
1.38	0.7098	4.76	40.1	4
1.02	0.7724	10.52	13.0	1
1.76	0.7744	13.45	13.0	Unfrac.

These results are in agreement with the absorption spectra of asphaltene thin films presented in figure (5.7). Both Fr.1 and Fr.4 have lower absorption in the visible part of light and therefore, will have lower photocurrent. The high fill factor in Fr.4 cell is a result of changing the sealant to lower thickness and easy to process; fastelfilm 230110 with 130 micrometer thick film, obtained from Fastel Adhesive.

Chapter: 6 Conclusion and recommendation

6.1 CONCLUSION

The essence of this research work is well encapsulated by the title of this work, namely, "*Asphaltene as light harvesting material in dye sentsized solar cell"*. Without a doubt the title is representative of the topics covered in this research. Despite the fact that there were considerable doubts about the suitability of these materials as sanitizer in DSSC at the start of this work, the research presented in this dissertation has comes a long way in removing many of these reservations. It has been proved that for at least one part of the asphaltene or asphaltene in whole can be effectively utilized. Asphaltene indeed is an excellent sanitizer in DSSC. In this regard, the present chapter concludes this dissertation by summarizing the motivation and the achievements of this research and recommending future work in this area.

Asphaltene the most abundant naturally forming material and undesirable part of crude oil that causes a lot of trouble to most oil refining companies has been shown in this study to be good sensitizer in DSSC. The results obtained show that every step in manufacturing the asphaltene cell has an effect on different cell parameters. According to results shown above, asphaltene solar cells have achieved a fill factor of 65% -70 %, when series resistance was minimized, Voc of 0.7 – 0.8 volt, and photocurrent of 10 - 13.69 mA/ cm^2 when UV-O treatment were employed and contaminates were eliminated. Therefore, a total overall efficiency of 4.55 % – 7.0 % could be easily attained with good engineering design and material process. Fraction three (Fr.3) obtained at 90/10 pentane to toluene ratio has produced the best asphaltene solar cell so far with 1.8 total efficiency. Un-fractionated asphaltene produced comparable result with fraction three.

6.2 FUTURE WORK

While our attention in this study was focused on perfecting the asphaltene solar cell by improving the photo-electrode there still more work can be done on the counter electrode. Good adhesion of the Pt layer onto the TCO substrate is very important for DSCs. If the Pt does not stick to the substrate, it may adsorb at the TiO_2 surface and catalyze dark currents at the TiO_2/electrolyte interface. Previous studies of DSCs constructed with different Pt electrodes show that, the short circuit currents with sputtered Pt electrodes had higher currents than those with Pt electrodes made by thermal decomposition of H2PtCl6 implemented in this study. This can be explained by better adhesion of the sputtered layers. A similar experiment showed that, especially for thick Pt layers, the adhesion is improved by heating the substrate during sputtering.

Another exercise attractive from a fundamental viewpoint is chemical characterization and molecular modeling of the various asphaltene fractions. In this regard, two techniques can be employed SAXS and WAXS. SAXS will give information about the shape and size of different asphaltene fraction. It is capable of delivering structural information of macromolecules between 5 and 25 nm, and therefore will help improves design and control of asphaltene cells. WAXS data help identifying aggregate on an inter-molecular level and thus well in identifying the optimal asphaltene concentration. Obtaining this data could be very useful information for subsequent studies with this material in such purpose.

Although the only fractionation procedure employed in this study was with varying pentane ratio with toluene, other solvents could be used and may produce better fraction. Methylene chloride as example has been utilized as dissolving medium of asphaltene and used with heptanes to fractionate the asphaltene. Varying the carbon ratio of fluctuating solvent may produce different asphaltene fraction with better physical properties suitable for DSSC.

Higher-power conversion efficiencies can be achieved by further optimizing the device structure. In a multi-component device like DSSCs, the overall performance of the cell depends critically on the individual properties of the constituent components and processes. Optimal performance is obtainable only when one understands the factors that control each of the components and depends on the ability to tune to the required configuration. The following chart is especially designed to represent the main components of asphaltene DSSC and to address parameters that one needs to deal with when trying to improve its performance.

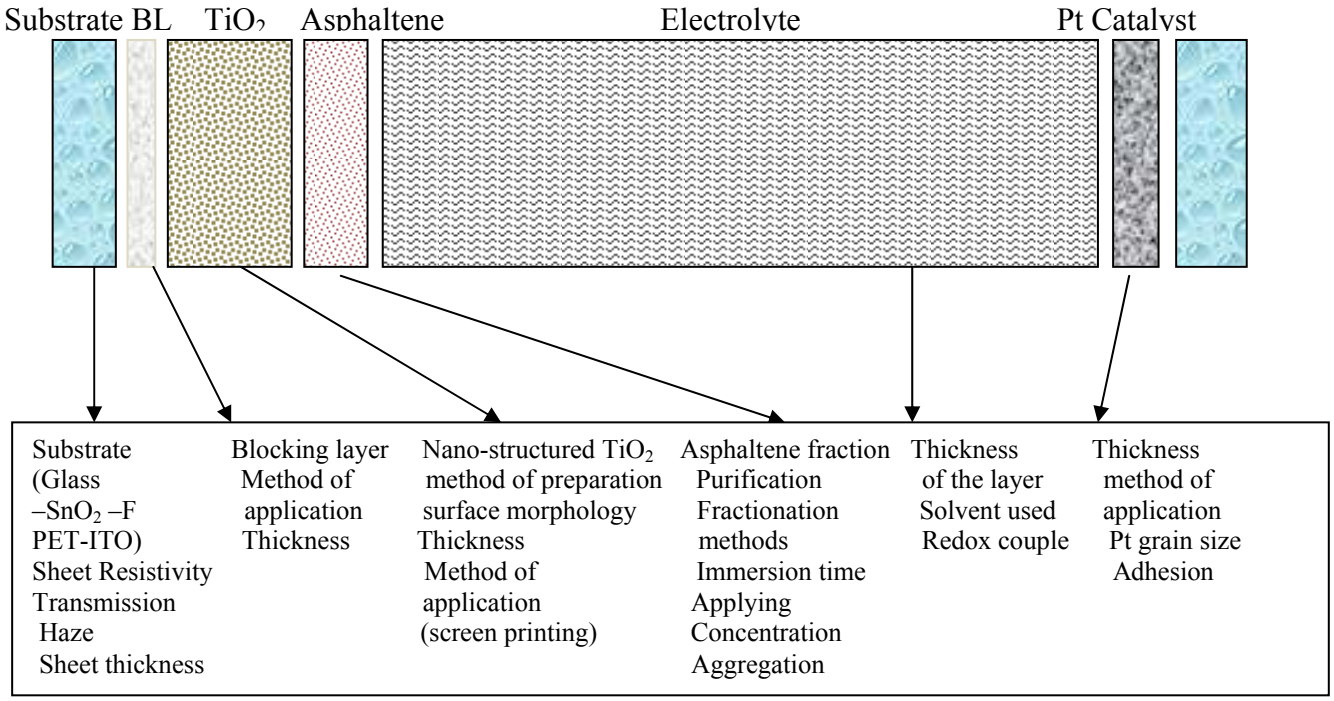

Illustration: 6.1 main components of asphaltene DSSC and Parameters to be considered to improve its performance

References

1. **The Energy Information Administration (EIA).** *International Energy Outlook 2010.* s.l. : U.S Department of Energy , 2010.

2. **Energy Information Administration.** *Emission of Greenhouse Gases in the United States 1985-1990.* Washigton Dc. : EIA, 1993. DOE/EIA-0573 .

3. **Pachauri, R.K. and Reisinger, A. (Eds.).** *Synthesis Report Summary for Policymakers.* Geneva, Switzerland. pp 104 : Intergovernmental Panel on Climate Change, 2007.

4. **Phillips, Tony.** *First Ever STEREO Images of the Entire Sun".* s.l. : NASA. , 6 February 2011. Retrieved 7 March 2011.

5. **Basu, S. and Antia, H. M.** "Helioseismology and Solar Abundances". *Physics Reports .* 2008, Vol. 457, (5–6).

6. **NASA.** *"Sun". World Book.* 2009.

7. **Materials, American Society for Testing and.** *ASTM G 173-03. Standard Tables for Reference Solar Spectral Irradiances: Direct Normal and Hemispherical for a 37° Tilted Surface.* West Conshohocken, PA : American Society for Testing and Materials, 2003.

8. **Pitjeva, E.V. and Standish, E.M.,.** "Proposals for the masses of the three largest asteroids, the Moon-Earth mass ratio and the astronomical unit. *Celestial Mechanics and Dynamical Astronomy.* 2009, Vols. 103, pp. 365-372.

9. **P. Foukal, C. Fröhlich, H. Spruit and T. M. L. Wigley.** Variations in solar luminosity and their effect on the Earth's climate. *Nature.* 2006, Vols. 443, 161-166.

10. **J. Wright, R. Perez and Michalsky, J.** Luminous Efficacy of Direct Irradiance: Variations with Insolation and Moisture Conditions,. *Solar Energy.* 1989, Vol. 42, 387-394.

11. **Würfel, Peter.** *The Physics of Solar Cells.* s.l. : Weinheim:Wiley-VCH. , 2005. ISBN 3527408576..

12. **NASA.** *NASA Surface meteorology and solar Energy .* s.l. : eosweb.larc.nasa.gov/sse/,, release 6.0, . last accssed may 1 2011.

13. *Polycrystalline Thin Film Solar Cell Technologies.* Colorado U.S.A : National Renewable Energy Laboratory, 2011.

14. **Green, M.A., et al.** "Very high efficiency silicon solar cells-science and technology. *IEEE Transactions on Electron Devices.* 1999, Vol. 46: 1940.

15. **Cusano, D. A.** CdTe Solar Cells and PV Heterojunctions in II-VI Compounds . *Solid State Electronics.* 6: 217., 1963, Vol. 6: 217.

16. **N. Naghavi, S. Spiering, M. Powalla, B. Cavana, D. Lincot.** High-efficiency copper indium gallium diselenide (CIGS) solar cells . *Progress in Photovoltaics: Research and Applications.* November 2003, Vol. 11, 7.

17. **Troshin, P. A Lyubovskaya, R. N.and Razumov, V. F.** Organic Solar Cells: Structure, Materials,Critical Characteristics, and Outlook. . *Nanotechnologies in Russia, .* 2008,, Vol. 3, 5-6.

18. **Shaheen, S. E. Ginley, D. S. Jabbour, G. E.** Organic-based photovoltaics:Toward low-cost power generation . *Materials Research Society bulletin* . 2005, Vol. 30 , 1.

19. **Kalowekamo, J. and Baker, Erin..** Estimating the manufacturing cost of purely organic solar cells. *Solar Energy.* 209, Vol. 83 .

20. **Brabec., Christoph J.** Organic photovoltaics: technology and market . *Solar Energy Materials & Solar Cells* . 2004, Vol. 83.

21. **M. Gratzel.** Dye-sensitized solar cells. *journal of Photochemistry Photobiology, C.* 2003, Vol. 4.

22. **Ruiz-Morales Y., and. Mullins, O. C.** Electronic Absorption Edge of Crude Oils and Asphaltenes Analyzed by Molecular Orbital Calculations with Optical Spectroscopy. *Energy & Fuels.* 2007, Vol. 21, pp. 944-952.

23. **Salmanova, Ch. K. Akhmedbekova, S. F. Mamedov, A. P. Kyazimov, S. M. and Abdulova, Sh.** Transformation of resins and asphaltene in photoirradiation. *Chemistry and Technology of Fuels and Oils.* 2007, Vol. 43, 5, pp. 415-421.

24. **Jiqian Wang, Chuan Li, Longli Zhang, Guohe Que, and Zhaomin Li.** The Properties of Asphaltenes and Their Interaction with Amphiphiles. *Energy Fuels* . 2009, Vol. 23, 7, pp. 3625–3631.

25. **Mullins, O.C., Sheu, E.Y., Hammami, A., and Marshall, A.** *Asphaltenes. Heavy oils, and petroleomics.* s.l. : Springer, 2007.

26. **Siffert, B., Kuczinski, J. and Papirer, E.** *Relationship between electrical charge and flocculation of heavy oil distillation residues in organic medium.* s.l. : Journal of Colloid Interface Science, 1990. pp. 107–117. Vol. 135.

27. **Neves, G. B. M. de Sousa, M. A. Travalloni-Louvisse, A. M., Lucas, E. F. and Gonz´alez, G.** Characterization of asphaltene particles by light scattering and electrophoresis. *Petroleum Science and Technology.* 2001, Vol. 19, pp. 35–43.

28. **Murray R. Gray, Grant Assenheimer, Lisa Boddez, and William C. McCaffrey.** Melting and Fluid Behavior of Asphaltene Films at 200-500 °C . *Energy & Fuels* . 2004, Vol. 18 .

29. **Andersen, S.I.** Effect of Precipitation Temperature on the Composition of n-Heptane Asphaltenes. *Fuel Science and Technology International.* 1994, Vol. 12, 1.

30. **Altgelt K. H. and Boduszynski, M. M.** *Composition and Analysis of Heavy Petroleum Fractions.* . New York : Marcel Dekker, 1994.

31. **Miller, J. T. Fisher, R. B. Thiyagarajan, P. Winans, R. E. Hunt, J. E.** Subfractionation and Characterization of Mayan Asphaltene. *Energy Fuels.* 1998, Vol. 12.

32. **McLean J. D., Kilpatrick, P. K.** Comparison of Precipitation and Extrography in the Fractionation of Crude Oil Residual. *Energy and Fuels.* 1997, Vol. 11.

33. **Brons G., Yu, J. M.** Solvent Deasphalting Effects on Whole Cold Lake Bitumen . *Energy & Fuels* . 1995 , Vol. 97, 4.

34. **Ouchi, K.** Correlation of aromaticity and molecular weight of oil asphaltene and preasphaltene. *Fuel* . 1985, Vol. 64.

35. **Calemman, V. Iwanski, P. Nali, M. Scotti, R. Montanari, L.** Structural Characterization of Asphaltenes of Different Origins . *Energy & Fuels.* 1995 , Vol. 9, 2.

36. **Bergmann, U. Mullins, C. and Cramer, S. P.** X-ray Raman Spectroscopy of Carbon in Asphaltene: Light Element Characterization with Bulk Sensitivity. *Analytical Chemistry.* 2000 , Vol. 72, 11.

37. **Speight, J. G.** *The Chemistry and Technology of Petroleum.* . New York : Marcel Dekker Inc, 1991.

38. **Mitra-Kirtley, S.,Mullins, O.C., Ralston, C.Y., Sellis, D. and Pareis C.,.** Determination of sulfur species in asphaltene, resin, and oil fractions of crude oils. *Applied Spectroscopy.* 1998, Vol. 52, 12.

39. Determination of sulfur species in asphaltene, resin, and oil fractions of crude oils. *Applied Spectroscopy.* 1998, Vol. 52, 12.

40. **Yen, T.F.,.** Structure of petroleum asphaltene and its significance. *Energy Sources* . 1974, Vol. 1, 4.

41. **Waldo, G. S. Mullins, O. C and Penner-Hahn, J. E. Cramer, S. P.** Determination of the Chemical Environment of Sulfur in Petroleum Asphaltenes by X-Ray Absorption-Spectroscopy. *Fuel.* 1992, Vol. 71.

42. **Moschopedis, S.E., Fryer, J.F., Speight, J.G.** Investigation of asphaltene molecular weights. *Fuel.* 1976, Vol. 55, pp. 227– 232.

43. **Schmitter, J.M., Ignatiadis, I., and Arpino, P.J.** Distribution of diaromatic nitrogen bases in crude oils. *Geochimica et Cosmochimica Acta.* November 1983, Vol. 47, 11,, pp. 1975-1984.

44. **Jacobson, J.M. Gray, M.R.** The use of infrared spectroscopy and nitrogen titration data in structural group analysis of bitumen. *Fuel.* 1978, Vol. 66, pp. 749-752.

45. **Mitra-Kirtley, S.,Mullins, O.C., Ralston, C.Y., Sellis, D. and Pareis C.** Determination of sulfur species in asphaltene, resin, and oil fractions of crude oils. *Applied Spectroscopy.* 1998, Vol. 52, 12, p. 1522.

46. **Clerc, R.J. and O'Neal, M.J.** The Mass Spectrometric Analysis of Asphalt: A Preliminary Investigation. *Analytical Chemistry.* 1961, Vol. 33, 3, pp. 380–382.

47. **Moschopedis, S.E. and Speight, J.G.** Preprints Division of Petroleum Chemistry. *American Chemical Society.* 1979,, Vol. 24, 4, p. 1007.

48. **Spiecker, P. M. Gawrys, K. L. Kilpatrick, P. K.** Aggregation and solubility behavior of asphaltenes and their sub-fractions,. *Journal of Colloid and Interface Science.* 2003, Vol. 267, 1, pp. 178-193.

49. **McLean J. D., Kilpatrick, P. K.,.** Comparison of Precipitation and Extrography in the Fractionation of Crude Oil Residua,. *Energy and Fuels.* 1997, Vol. 11, pp. 570-585.

50. **Kaminski, T. J, Fogler, H. S, Wolf, N, Wattana, P, Mairal, A.** Classification of asphaltenes via fractionation and the effect of heteroatom content on dissolution kinetics. *Energy & Fuels,.* 2000,, Vol. 14, 1, pp. 25-30.

51. **Yang, X. L. Hamza, H. Czarnecki, J.** Investigation of sub-fractions of Athabasca asphaltenes and their role in emulsion stability. *Energy & Fuel.* 2004, Vol. 18, 3, pp. 770- 777.

52. **Ali, M. F, Perzanowski, H. Bukhari, A, Al-Haji, A. A.** Nickel and Vanadyl Porphyrins in Saudi Arabian Crude Oils. *Energy & Fuels.* 1993, Vol. 7, 2, pp. 179-184.

53. **Pena, M. E. Manjarrez, A. Campero, A.** Distribution of Vanadyl porphyrins in a Mexican offshore heavy crude oil. *Fuel Processing Technology* . 1996, Vol. 46, 3, pp. 171-182.

54. **Chouparova, E, Lanzirotti, A, Feng, H, Jones, K. W, Marinkovic, N, Whitson, C. Philp, P.** Characterization of petroleum deposits formed in aproducing well by synchrotron radiation based microanalyses. *Energy Fuels.* 2004, Vol. 18, 4, pp. 1199-1212.

55. **Speight, J. G.** *The Chemistry and Technology of Petroleum.* New York : Marcel Dekker, Inc., 2006.

56. **Calemman, V. Iwanski, P. Nali, M. Scotti, R. Montanari, L.** Structural Characterization of Asphaltenes of Different Origins. *Energy Fuels.* 1995, Vol. 9, 2, pp. 225-230.

57. **Groenzin, H. and Mullins, O. C.** Molecular Size and Structure of Asphaltenes from various Sources. *Energy Fuels.* 2000, Vol. 14, pp. 677-684.

58. **Chianelli, R. R., Siadati, M., Mehta, A. Pople, J. Ortega, L. C., and Chiang, L. Y.** Self-Assembly of Asphaltene Aggregates:Synchrotron,Simulation and Chemical Modeling Techniques Applied to Problems in the Structure and Reactivity of Asphaltenes. [book auth.] O. C., Sheu, E. Y., Hammami, A. Mullins. [ed.] A. G., Eds Marshall. *AsphalteneHeavy Oils and Petroleomics.* New York : .; Springer, 2007, p. Chapter 15.

59. **Yen, T. F. Erdman, J. G., and Pollack, S. S.** Investigation of Structure of Petroleum Asphaltenes By X-Ray Diffraction. *Analytical Chemistry.* 1961, Vol. 33, 11, pp. 1587-1594.

60. **Andersen, S. I. Birdi, K. S.** Aggregation of Asphaltenes as Determined by Calorimetry. *Journal of Colloid and Interface Science.* 1991, Vol. 142, 2, pp. 497-502.

61. **Pomerantz, A. E. Hammond, M.R. Morrow, A. L., Mullins, O. C. and Zare, R. N.** Two-Step Laser Mass Spectrometry of Asphaltenes. *Journal American Chemical Society.* 2008, Vol. 130, 23, pp. 7216–7217.

62. **Shea, R.C., Habicht, S. C., Vaughn, W. E., and Kenttämaa, H. I.** Design and Characterization of a High-Power Laser-Induced AcousticDesorption Probe Coupled with a Fourier Transform Ion Cyclotron Resonance Mass Spectrometer. *Analytical Chemistry.* 2007, Vol. 79, 7, pp. 2688–2694.

63. **Ravey, J.C., Ducouret, G., Espinat, D.,.** "Asphaltene macrostructure by small angle neutron scattering". *fuel.* 1988, Vol. 67, p. 1560.

64. **Rajagopal, K. and Silva, S. M. C.** An experimental study of asphaltene particle sizes in n-heptane-toluene mixtures by light scattering. *Brazilian Journal of Chemical Engineering.* 2004, Vol. 21, 4, pp. 601-609.

65. **Acevedo, S., Escobar, G. Ranaudo, M. A. Pinate, J. Amorin, A. Diaz, M. and Silva, P.** Observations about the structure and dispersion of petroleum asphaltenes aggregates obtained from dialysis fractionation and characterization. 1997, Vol. 11, 4, pp. 774-778.

66. **E.B., Sirota.** Physical Structure of Asphaltenes. *Energy Fuel.* 2005, Vol. 19, 4, pp. 1290-1296.

67. **Cyr, N. McIntyre, D. D. Toth, G. Strausz, O. P.** "Hydrocarbon Structural Group Analysis of Athabasca Asphaltene and its G.P.C. Fractions by C-13 N.M.R.,. *Fuel,.* 1987, Vol. 66, pp. 1709-1714.

68. **Jacobs, F. S, Filby, R. H.** Liquid Chromatographic Fractionation of Oil-Sand and Crude Oil Asphaltenes,. *Fuel.* 1983, Vol. 62, 10, pp. 1186-1192.

69. **Andersen, S. I. Keul, A. Stenby, E.** Variation in composition of sub-fractions of petroleum asphaltenes. *Petroleum Science Technology .* 1997, Vol. 15, (7-8), pp. 611-645.

70. **Fenistein, D., Barre, L.** Experimental measurement of the mass distribution of petroleum asphaltene aggregatessmall-angle X-ray scattering using ultracentrifugation and. *Fuel.* 2001, Vol. 80, 2, pp. 283-287.

71. **Yarranton, H. W. Alboudwarej, H. Jakher, R.** Investigation of asphaltene association with vapor pressure osmometry and interfacial tension measurements. *Industrial & Engineering Chemistry Research.* 2000, Vol. 39, 8, pp. 2916-2924.

72. **Yarranton, H. W. Masliyah, J. H.** Molar Mass Distribution and Solubility Modeling of Asphaltenes. *AICHE Journal.* 1996, Vol. 42, 12, pp. 3533-3543.

73. **Groenzin, H. Mullins, O. C. Eser, S. Mathews, J. Yang, M. G. Jones, D.,.** Molecular size of asphaltene solubility fractions. *Energy & Fuels.* 2003, Vol. 17, 2, pp. 498-503.

74. **Buenrostro-Gonzalez, E. Andersen, S. I. Garcia-Martinez, J. A. Lira-Galeana, C.** Solubility/molecular structure relationships of asphaltenes in polar and nonpolar media. *Energy Fuels.* 2002, Vol. 16, 3, pp. 732-741.

75. **Nalwaya, V. Tangtayakom, V. Piumsomboon, P. Fogler, S.** Studies on asphaltenes through analysis of polar fractions. *Industrial & Engineering Chemistry Research.* 1999, Vol. 38, 3, pp. 964-972.

76. **Murgich, J.** Intermolecular forces in aggregates of asphaltenes and resins. *Petroleum Science and Technology.* 20 2002, Vol. 20, 9-10, pp. 983-997.

77. **Porte, G. Zhou, H. G. Lazzeri, V.** Reversible description of asphaltene colloidal association and precipitation. *Langmuir, 2003, 19 (1), pp 40–47.* 2003, Vol. 19, 1, pp. 40-47.

78. **Murgich, J. Abanero, J. A. Strausz, O. P. ".** Molecular recognition in aggregates formed by asphaltene and resin molecules from the Athabasca oil sand. *Energy & Fuels.* 1999, Vol. 13., 2, pp. 278-286.

79. **Sharma, A. Groenzin, H. Tomita, A. Mullins, O. C.** Probing order in asphaltenes and aromatic ring systems by HRTEM. *Energy & Fuels.* 2002, Vol. 16, 2, pp. 490-496.

80. **Murgich, J.** "Molecular simulation and the aggregation of the heavy fractions in crude oils,. *Molecular Simulation.* 2003, Vol. 29, 6-7, pp. 451-461.

81. **Sheremata, J. M. Gray, M. R. Dettman, H. D. McCaffrey, W. C.** "Quantitative molecular representation and sequential optimization of athabasca asphaltenes,. *Energy & Fuels.* 2004, Vol. 18, 5, pp. 1377-1384.

82. **Strausz, O. P. Mojelsky, T. W. Lown, E. M.** The Molecular-Structure of Asphaltene - an Unfolding Story. *Fuel.* 1992, Vol. 71, 12, pp. 1355-1363.

83. **Yi-Qiao Song H. Z, Johnson, D. L. and Mullins, O. C.** Critical Nanoaggregate Concentration of Asphaltenes by Direct-Current (DC) Electrical Conductivity. *Energy & Fuels.* 2009, Vol. 23, pp. 1201–1208.

84. **Andersen, S. I. Birdi, K. S.** Aggregation of Asphaltenes as Determined by Calorimetry. *journal of Colloid Interface Science .* 1991, Vol. 142, pp. 497-502.

85. **Becquerel, A. E, Smith, W.** 1839, Comptes Rendus de l'Acad´emie des Sciences, Vol. 9, p. 561.

86. **Smith, W.** 1873, Nature , Vol. 7, p. 303.

87. **Adams, W. G. Day,R. E.** 1876. Proceedings of the Royal Society London. Vol. 25, p. 113.

88. **Einstein, A.** 1905, Annalen der Physik, Vol. 17, p. 132.

89. **Czochralski, J. Z.** 1918, Physical Chemistry, Vol. 92, p. 219.

90. **Chapin, D. M. Fuller, C. S. and Pearson G. L.** A New Silicon p-n Junction Photocell for Converting Solar Radiation into Electrical Power. *Journal of Applied Physics.* 1954, Vol. 25, 5, pp. 676–677.

91. **Green, M. A.** Progress Photovoltaic's:. *Research and Applications.* 1994, Vol. 2, p. 87.

92. **Shi, Z. Wenham, S. R.** Progress Photovoltaic. *Research and Applications.* 1994, Vol. 2, p. 153.

93. **Pochettino, A.** 1906, Academy Lincei Rendus, Vol. 15 , p. 355.

94. **Volmer, M.** 1913 , Annales Physik, Vol. 40, p. 775.

95. **Borsenberger, P.M. Weiss,.** *Organic Photoreceptors for Imaging Systems.* s.l. : Marcel Dekker, 1993 .

96. **Bube, R.H.** *Photoconductivity of Solids* **.** New York : Wiley , 1960.

97. **West, W.** Proceedinds of the Vogel Centennial Symposium. *Photography Science and Engineering.* 1974, Vol. 18.

98. **Moser, J.** 1887, Monatshefte für Chemie / Chemical Monthly, Vol. 8 , p. 373.

99. **Rigollot, H. C. R.** Paris : s.n., 1893 , Academic Science , Vol. 116 , p. 561.

100. **Gerischer, H. and Tributsch, H. Ber. Bunsenges.** 1968 , Physical Chemistry , Vol. 72, p. 437.

101. **O'Regan B., Grätzel M.** A low cost high-efficiency solar cell based on dye-sensitized colloidal TiO2 films. *Nature.* 1991, Vol. 353, pp. 737-740.

102. **Nazeeruddin, M. K. Kay, A. Rodicio, I. Humphry-Baker, R Mueller, E. Liska, P. Vlachopoulos, N., M.** Conversion of Light to Electricity by cis-X2Bis(2,2'-bipyridyl-4,4'-dicarboxylate)ruthenium(II) Charge-Transfer Sensitizers (X = Cl-, Br-, I-, CN- and SCN-) on Nanocrystalline TiO2 Electrodes. *Journal of American chemical Society.* 1993, Vol. 115, pp. 6382-6390.

103. **Nogueira, A.F. Longo, C. and De Paoli, M.A.** 2004, Coordination Chemistry Review. , Vol. 248, p. 1455.

104. **Grätzel, M.** Dye-sensitized solar cells Review. *Journal of Photochemistry and Photobiology C: Photochemistry Reviews.* 2003, Vol. 4, pp. 145–153.

105. **Kyrylyuk, A. V., et al.** s.l. : (Nature Publishing Group):, 2011, Nature Nanotechnology .

106. **Olsen, E. Hagen G. and Lindquist, S. E.** 2000., Solar Energy Material Solar Cells, , Vol. 63 , pp. 267-273.

107. **Kitamura, T. Maitani, M. Matsuda, M. Wada Y. and Yanagida, S.** Improved solid-state dye solar cells with polypyrrole using a carbon-based counter electrode. *Chemical Letter.* Vol. 10, pp. 1054-1055.

108. **Joseph D. Roy-Mayhew, David J. Bozym, Christian Punckt, and Ilhan A. Aksay.** Functionalized Graphene as a Catalytic Counter Electrode in Dye-Sensitized Solar Cells. *ACS Nano.* 2010, Vol. 4, 10, pp. 6203–6211.

109. **Sapp, S.A. Elliott, C.M. Contado, C. Caramori, S. Bignozzi, C.A.** Substituted Polypypridine Complexes of Cobalt(II/III) as Efficient Electron-Transfer Mediators in Dye-Sensitized Solar cells. *Journal of the American Chemical Society.* 2002, Vol. 124, pp. 11215-11222.

110. **Kelly C. A. and Meyer, G. J.** Excited state processes at sensitized nanocrystalline thin film semiconductor interfaces. *Coordination Chemistry Review.* 2001, Vol. 211, pp. 295-315.

111. **Tennakone, K. Kumara, G. R. R. Kottegoda I. R. M. and Perera, V. P. S.** An efficient dye-sensitized photoelectrochemical solar cell made from oxides of tin and zinc. *Chemical Communication.* 1999, Vols. 15-16.

112. **Sayama, K., Sugihara, H. Arakawa, H.** Photoelectrochemical properties of a porous Nb2O5 electrode sensitized by a ruthenium dye. *Chemistry of Materials.* 1998, Vol. 10, 12, pp. 3825-3832.

113. **Kalyanasundaram, K. and Gratzel, M.** Applications of functionalized transition metal complexes in photonic and optoelectronic devices. *Coordination Chemical Review.* 1998, Vol. 177, pp. 347-414.

114. **Park, N. G. van de Lagemaat, J. and Frank, A.** Comparison of Dye-Sensitized Rutile- and Anatase-Based TiO2 Solar Cells. *Journal of Physical Chemistry B.* 2000., Vol. 104, 38, pp. 8989-8994.

115. **Vlachopoulos, N. Liska, P. Augustynski, J. and Graetzel, M.** Very efficient visible light energy harvesting and conversion by spectral sensitization of high surface area polycrystalline titanium dioxide films. *Journal of American Chemical Society.* 1988, Vol. 110, pp. 1216-1220.

116. **Ellingson, R. J. Asbury, J. B. Ferrere, S.H. Ghosh, N. Sprague, J. R. Lian T. and Nozik, A. J.** "Dynamics of electron injection in nanocrystalline titanium dioxide films sensitized with [Ru(4,4'-dicarboxy-2,2'- bipyridine)2(NCS)2] by infrared transien absorption. *Journal of Physical Chemistry. B.* 1998, Vol. 102, pp. 6455-6458.

117. **Hart, J. N. Menzies, D. Cheng, Y.-B Simon G. P. and Spiccia, L.** TiO2 sol–gel blocking layers for dye-sensitized solar cells. *Comptes Rendus Chimie.* May-June 2006,, Vol. 9, 5-6, pp. 622-626.

118. **Ito, S. Ishikawa, K. Wen, C.-J. Yoshida S. and Watanabe, T.** Dye-Sensitized Photocells with Meso-Macroporous TiO2 Film Electrodes. *Bulletin Chemical Society of Japan.* 2000, Vol. 73, 11, pp. 2609-2614.

119. **Mor, G. K. Shankar, K. Paulose, M. Varghese, O. K and Grimes, C. A.** 2006, Nontechnology Letters, Vol. 6, pp. 215-218.

120. **Jiu, J. Isoda, S. Wang F. and Adachi, M.** Dye-Sensitized Solar Cells Based on a Single-Crystalline TiO2 Nanorod Film. *Journal of Physical Chemistry. B.* 2006, Vol. 110, p. 2087 2092.

121. **Murakoshi, K. Kano, G. Wada, Y. Yanagida, S. Miyazaki, H. Matsumoto, M. and Murasawa, S. J.** Importance of binding states between photosensitizing molecules and the TiO2 surface for efficiency in a dye-sensitized solar cell. *Electroanalitcal Chemistry.* 1995, Vol. 396, pp. 27-34.

122. **Nazeeruddin, M. K. Klein, C. Liska P. and Graetzel, M.** Synthesis of novel ruthenium sensitizers and their application in dye-sensitized solar cells. *Coordinatation Chemical Review.* 2005, Vol. 249, pp. 1460-1467.

123. **Gillaizeau-Gauthier, F. Odobel, M. Alebbi, R. Argazzi, E. Costa, C. A. Bignozzi, P. Qu and G. J. Meyer.** Phosphonate-Based Bipyridine Dyes for Stable Photovoltaic Devices. *Inorganic Chemistry.* 2001, Vol. 40, pp. 6073-6079.

124. **Zabri, H. Gillaizeau, I. Bignozzi, C. A. Caramori, S. Charlot, M.-F Cano-Boquera . J. and J. and Odobel, F. ,.** Synthesis and Comprehensive Characterizations of New cis-RuL2X2 (X = Cl, CN, and NCS) Sensitizers. *Inorganic Chemistry.* 2003, Vol. 42, 21, pp. 6655-6666.

125. **Altobello, S. Bignozzi, C. A. Caramori, S. Larramona, G.S. Marzanni, Quici, G. and.** Sensitization of TiO2 with ruthenium complexes containing boronic acid functions. 2004, Vol. 166, 1-3, pp. 91-98.

126. **Ford, W. E. and Rodgers, M. A. J.** Interfacial Electron Transfer in Colloidal SnO2 Hydrosols Photosensitized by Electrostatically and Covalently Attached Ruthenium(II) Polypyridine Complexes. *Journal of physical chemistry.* 1994, Vol. 98, pp. 3822-3831.

127. **Fox, M. A. Nobs, F. J. and Voynick, T. A.** Chemically modified electrodes in dye-sensitized photogalvanic cells. *Journal of American Chemical Society,.* 1980, Vol. 102, 12, pp. 4036-4039.

128. **Zou, C. and Wrighton, M. S.** Synthesis of octamethylferrocene derivatives via reaction of (octamethylferrocenyl)methyl carbocation with nucleophiles and application to functionalization of surfaces. *The Journal of American Chemical Society.* 1990, Vol. 112, 21, pp. 7578-7584.

129. **Polo, A. S. Itokazu, M. K and Murakami Iha, N. Y.** Metal complex sensitizers in dye-sensitized solar cells. *Coordination Chemistry Reviews.* 2004, Vol. 248, 13-14, pp. 1343-1361.

130. **Hagfeldt, A. and Graetzel, M.** Molecular Photovoltaics. *Accounts of Chemical Research,.* 2000, Vols. 33,, 5, pp. 269-277.

131. **Gratzel, M.** Conversion of sunlight to electric power by nanocrystalline dye-sensitized solar cells. *Journal of Photochemistry Photobiology.* 2004, Vol. 164, 1-3, pp. 3-14.

132. **Kong, F.T. Dai, S.Y. and Wang, K.J.** New Amphiphilic Polypyridyl Ruthenium(II) Sensitizer and Its Application in Dye-Sensitized Solar Cells. *Chinese Journal of Chemistry.* 2007, Vol. 25, 2, pp. 168-171.

133. **Schmidt-Mende, L. Bach, U. Humphry-Baker, R. Horiuchi, T. Miura, Ito, H. S. Uchida, S.and Graetzel, M.** Organic dye for highly efficient solid-state dye-sensitized solar cells. *Advanced Materials.* 2005., Vol. 17, 7, pp. 813-815.

134. **Tokuhisa, H. and Hammond, P. T.** Solid-State Photovoltaic Thin Films using TiO2, Organic Dyes, and Layer-by-Layer Polyelectrolyte Nanocomposites. *Advanced Functional Materials.* 2003, Vol. 13, 11, pp. 831-839.

135. **Giribabu, L. Kumar, C. V. Reddy, V. G. Reddy, P. Y. Rao, C. S. Jang, S.R. Yum, J.-H.Nazeeruddin, M. K. and Graetzel, M.** Unsymmetrical alkoxy zinc phthalocyanine for sensitization of nanocrystalline TiO2 films. *Solar Energy Materials Solar Cells.* 2007, Vol. 91, 17, pp. 1611-1617.

136. **Hara, K. Sayama, K. Arakawa, H. Ohga, Y. Shinpo, A. and Suga, S.** A coumarin-derivative dye sensitized nanocrystalline TiO2 solar cell having a high solar-energy conversion efficiency up to 5.6%. *Chemical Communication,.* 2001,, 6, pp. 569-570.

137. **Hara, K. Kurashige, M. Dan-oh, Y. Kasada, C. Shinpo, A. Suga, S. Sayama, K.and Arakawa, H.** Design of new coumarin dyes having thiophene moieties for highly efficient organic-dye-sensitized solar cells. *New Journal of Chemistry.* 2003,, Vol. 27, 5, pp. 783-785.

138. **Sayama, K. Tsukagoshi, S. Mori, T. Hara, K. Ohga, Y. Shinpou, A. Abe, Y. Suga, S. and Arakawa, H.** Efficient sensitization of nanocrystalline TiO2 films with cyanine and merocyanine organic dyes,. *Solar Energy Material Solar Cells.* 2003, Vol. 80, 1, pp. 47-71.

139. **Clifford, J. N. Palomares, E. M. Nazeeruddin, K. Thampi, R. Graetzel, M. and Durrant, J. R.** Multistep Electron Transfer Processes on Dye Co-sensitized Nanocrystalline TiO<sub>2<sub> Films. *Journal of American Chemical Society.* 2004, Vol. 126, 18, pp. 5670-5671.

140. **Fang, J. Su, L. Wu, J. Shen, Y. and Lu, Z.** The photoresponse properties of nanocrystalline TiO2 particulate film co-modified with dyes. *New Journal of Chemistry,.* 1997, Vol. 21, 6/7, pp. 839-840.

141. **Tributsch, H.** Dye sensitization solar cells: a critical assessment of the learning curve. *Coordination Chemistry Review,.* 2004, Vol. 248, 13-14, pp. 1511-1530.

142. **Figgemeier, E. and Hagfeldt, A.** Are dye-sensitized nano-structured solar cells stable? An overview of device testing and component analyses. *International Journal of Photoenergy,.* 2004,, Vol. 6, 3, pp. 127-140.

143. **Argazzi, R. Bignozzi, C. A. Heimer, T. A. Castellano, F. N. and Meyer, G. J.** Light-Induced Charge Separation across Ru(II)-Modified Nanocrystalline TiO2 Interfaces with Phenothiazine Donors. *The journal of physical chemistry B.* 1997, Vol. 101, 14, pp. 2591-2597.

144. **Oskam, G. Bergeron, B. V. Meyer, G. J.and Searson, P. C.** Pseudohalogens for Dye-Sensitized TiO₂Photoelectrochemical Cells. *Journal of Physical chemistry. B,.* 2001,, Vols. 105,, 29, pp. 6867-6873.

145. **Wang, Z.S, Sayama, K and H. Sugihara,.** Efficient eosin Y dye-sensitized solar cell containing Br-/Br-3(-) electrolyte. *Journal of Physical chemistry B,.* 2005,, Vols. 109,, 47, pp. 22449-22455.

146. **Hamann, T. W. Jensen, R. A, Martinson, A. B. F. Van Ryswyk , H. and. Hupp, J. T.** Advancing beyond current generation dye-sensitized solar cells. *Energy Environmental Science,.* 2008,, Vol. 1, 1, pp. 66-78.

147. **Nusbaumer, H. Zakeeruddin, S. M. Moser, J.E. and Graetzel, M.** An Alternative Efficient Redox Couple for the Dye-Sensitized Solar Cell System. *Chemistry - A European Journal.* 2003, Vol. 9, 16, pp. 3756-3763.

148. **Cameron, P. J. Peter, L. M. Zakeeruddin, S. M. and Gratzel, M.** Electrochemical studies of the Co(III)/Co(II)(dbbip)2 redox couple as a mediator for dye-sensitized nanocrystalline solar cells. *Coordination Chemistry Reviews.* 2004, Vol. 248, 13-14, pp. 1447-1453.

149. **Ma, T. Fang, X. Akiyama, M. Inoue, K. Noma, H. and Abe, E.** Properties of several types of novel counter electrodes for dye-sensitized solar cells. *Journal of Electroaanalytical chemistry,.* 2004, Vol. 574, 1, pp. , 77-83.

150. **Kay, A. and Graetzel, M.** Low cost photovoltaic modules based on dye sensitized nanocrystalline titanium dioxide and carbon powder. *Solar Energy Material Solar Cells,.* 1996, Vol. 44, 1, pp. 99-117.

151. **Saito, Y. Kubo, W. Kitamura, T. Wada, Y. andYanagida, S.** I-/I-3(-) redox reaction behavior on poly(3,4-ethylenedioxythiophene) counter electrode in dye-sensitized solar cells. *Journal of Photochemistry Photobiology, A,.* 2004, Vols. 164,, 1-3, pp. 153-157.

152. **Wang, P. Zakeeruddin, S. M. Moser, J.E and Graetzel, M.** A New Ionic Liquid Electrolyte Enhances the Conversion Efficiency of Dye-Sensitized Solar Cells. *Journal of Physical chemistry B,.* 2003, Vols. 107,, 48, pp. 13280-13285.

153. **Matsumoto, H. Matsuda, T. Tsuda, T. Hagiwara, R. Ito, Y. and Miyazaki, Y.** The application of room temperature molten salt with low viscosity to the electrolyte for dye-sensitized solar cell. 2001, Vol. 1, pp. 26-27.

154. **Kubo, W. Kitamura, T. Hanabusa, K. Wada, Y. and Yanagida, S.** Quasi-solid-state dye-sensitized solar cells using room temperature molten salts and a low molecular weight gelator. *Chemical Communication.* 2002, pp. 374-375.

155. **Yum, J.-H. Jang, S.-r. Humphry-Baker, R. Graetzel, M., Cid, J.-J. Torres, T. and. Nazeeruddin, M. K.** Effect of coadsorbent on the photovoltaic performance of zinc pthalocyanine-sensitized solar cells. *Langmuir.* 2008, Vol. 24, 10, pp. 5636-5640.

156. **Khazraji, A.C, Hatchandani, S. Das, S. Kamat, P.** Controlling Dye (Merocyanine-540) Aggregation on Nanostructured TiO2 Films. An Organized Assembly Approach for Enhancing the Efficiency of Photosensitization. *Journal of Physical Chemistry B.* 1999, Vol. 103, 22, pp. 4693–4700.

157. **Kambe, S. Murakoshi, K. Kitamura, T. Wada, Y. Yanagida, S. Kominami, H. Kera, Y.** Mesoporous electrodes having tight agglomeration of single-phase anatase TiO2 nanocrystallites: Application to dye-sensitized solar cells. *Solar Energy Material Solar Cells.* 2000, Vol. 61, 1, pp. 427-441.

158. **Keis, K. Lindgren, J. Lindquist, S.E. Hagfeldt, A.** Studies of the Adsorption Process of Ru Complexes in Nanoporous ZnO Electrodes. 2000, Vol. 16, 10, pp. 4688–4694.

159. **Hirata, N.** Ph.D. Thesis, Imperial College, London, UK, 2005.

160. **Wenger, B. Grätzel, M. Moser, J.E.** Rationale for Kinetic Heterogeneity of Ultrafast Light-Induced Electron Transfer from Ru(II) Complex Sensitizers to Nanocrystalline TiO2. *Journal of American Chemical Society. .* 2005, Vol. 127, 35, pp. 12150–12151.

161. **Pellnor, M. Myllyperkiö, P. Korppi-Tommola, J. Yartsev, A. Sundström, V.** Photoinduced interfacial electron injection in RuN3 TiO2 thin films: Resolving picosecond timescale injection from the triplet state of the protonated and deprotonated dyes. *Chemistry physics letters. 462 (2008) 205.* 2008, Vol. 462 , 4-6, pp. 205-208.

162. **Nazeeruddin, M. K. and Gratzel, M.** Transition metal complexes for photovoltaic and light emitting applications. *Structure and Bonding.* 2007, Vol. 123, pp. 113-175 .

163. **Emery, Keith.** [ed.] Antonio Luque and Steven Hegedus. *Handbook of photovoltaic science and engineering.* Chichester : John Wiley & Sons Inc.,, 2003.

164. **Ancheyta, J. Centeno, G. Trejo,F. Marroquín,G. García, J. A. Tenorio,E. and A. Torres.** Extraction and Characterization of Asphaltenes from Different Crude Oils and Solvents. *Energy & fuel.* 2002, Vol. 16, 5, pp. 1121–1127.

165. **Seigo Ito, Peter Chen, Pascal Comte, Mohammad Khaja Nazeeruddin, Paul Liska,.** Fabrication of screen-printing pastes from TiO2 powders for dye-sensitised solar cells. *Progress in Photovoltaics : Research and applications.* 2007, Vol. 15, 7, pp. 603-612.

166. **S.Ito, P.Liska, P.Comte, R.Charvet, P.Pechy, U.Bach, L.Schmidt-Mende, S.M. Zakeeruddin, A.Kay, M.K. Nazeeruddin, M.Graetzel,.** Control of dark current in

photoelectrochemical(TiO2/I3) and dye-sensitized solar cells. *Chemical Communication* . 2005, pp. 4351–4353.

167. **W.Y.Gan, S.W.Lam,K.Chiang,R.Amal,H.Zhao,M.P.Brungs,.** Novel TiO2 thin film with non-UV activated super wetting and anti fogging behaviours,. *Journal of Material Chemistry* . 2007, Vol. 17, pp. 952–954.

168. **M.Thelakkat, C.Schmitz,H.-W.Schmidt,.** Fully Vapor-Deposited Thin Layer Titanium Dioxide SolarCells,. *Advanced Materials.* 2002, Vol. 14, pp. 577–581. .

169. **M.Okuya, K.Nakade,S.Kaneko,.** PorousTiO2 thin films synthesized by aspray pyrolysis deposition(SPD) technique and their application to dye-sensitized solar cells,. *Solar Energy Material Solar Cells.* 2002, Vol. 70, pp. 425–435.

170. **Hoshikawa, T. Yamada,M. Kikuchi,R. Eguchi. K.** Impedance analysis for dye-sensitized solar cells with a three-electrode system. *Journal of Electroanalytical Chemistry.* 2005, Vol. 577, pp. 339–348.

171. **Anneke. H, A. Georg.** Diffusion in the electrolyte and charge-transfer reaction atthe platinum electrode in dye-sensitized solar cells. *Electrochimica Acta.* 2001, Vol. 46, pp. 3457–3466.

172. **Weiqing. L., Linhua. H., Songyuan. D., Lei. G., Nianquan. J., Dongxing. K.** The effect of the series resistance in dye-sensitized solar cells explored by electron transport and back reaction using electrical and optical modulation. *Electrochimica Acta* . 2010, Vol. 55, pp. 2338–2343.

173. **Naoki K., Islam. A, Yasuo. C., Han. L.** Improvement of efficiency of dye-sensitized solar cells based on analysis of equivalent circuit. *Journal of Photochemistry and Photobiology A: Chemistry.* 2006, Vol. 182, pp. 296–305.

174. **Kun-Mu Leea, Vembu Suryanarayananb, Kuo-Chuan Hoc,.** High efficiency quasi-solid-state dye-sensitized solar cell based on polyvinyidene fluoride-co-hexafluoro propylene containing propylene carbonate and acetonitrile as plasticizers. *Journal of Photochemistry and Photobiology A: Chemistry* . 2009 , Vol. 207 , pp. 224–230.

175. **Hsueh-Pei Lu, Chen-Yuan Tsai, Wei-Nan Yen, Chou-Pou Hsieh, Cheng-Wei Lee, Chen-Yu Yeh and Eric Wei-Guang Diau.** Control of Dye Aggregation and Electron Injection for Highly Efficient Porphyrin Sensitizers Adsorbed on Semiconductor Films with Varying Ratios of Coadsorbate. *Journal of Physical Chemistry. C,* . 2009, Vol. 113, 49, pp. 20990–20997.

176. **Qing Wang, Wayne M. Campbell, Edia E. Bonfantani, Kenneth W. Jolley, David L. Officer,Penny J. Walsh, Keith Gordon, Robin Humphry-Baker, Mohammad K. Nazeeruddin, and Michael Grätzel.** Efficient Light Harvesting by Using Green Zn-Porphyrin-Sensitized Nanocrystalline TiO2 Films. *The journal of physical chemistry B.* 2005 109 (32), pp, Vol. 19, 32, pp. 15397–15409.

177. **Byoung-Kuk Lee, Jang-Joo Kim.** Enhanced efficiency of dye-sensitized solar cells by UV–O3 treatment of TiO2 layer. *Current Applied Physics.* 2009, Vol. 9, pp. 404–408.

178. **Dongshe Zhang, Tsukasa Yoshida, Torsten Oekermann, Ken Furuta,and Hideki Minoura.** Room-Temperature Synthesis of Porous Nanoparticulate TiO2 Films for Flexible Dye-Sensitized Solar Cells. *Advanced Functional Materials.* 2006, Vol. 16, p. 1228.

Abbreviations

GHG	Green house gasses
Btu	British thermal unit
EIA	Energy Information Administration
IPCC	Intergovernmental Panel on Climate Change (IPCC)
HFCs,	Hydrofluorocarbons
PFCs	Perfluorocarbons
SF6	Sulphur hexafluoride
GWP	Global warming potential
ASTM	American Society for Testing and Materials
G173-03	Global Terrestrial Reference Spectra
σ	Stefan Boltzmann constant (5.67 × 10−8 W/m2/K4).
S_O	Solar constant
AU	The astronomical unit (149,604,970 km)
DSE	Diameter of earth sphere
ASE	Surface area of earth sphere
AM1.5	Air Mass at 48^O zenith angle
AM 0	Air Mass at 0 zenith angle
UVR	Ultra violet radiation
AC	Earth cross-sectional area
TWh	TeraWatt hour
DSSC	Dye sensitized solar cell
C13-NMR	Carbon $_{13}$ nuclear magnetic resonance
XANES	X-ray absorption near-edge spectroscopy
IR	Infrared spectroscopy
ESR	Electron Spin resonance mass spectroscopy,

VPO	Vapor pressure osmometry
GPC	Gel permeation chromatography
MS	Mass spectrometry
SEC	Size exclusion chromatography
SAXS	Small angle X-ray scattering
SANS	Small angle neutron scattering
Amu	Atomic mass unit
L2MS	Two-step laser desorption ionization mass spectrometry
LIAD	laser-induced acoustic desorption
FFTEM	Freeze-fracture-transmission electron-microscopy
WAXS	Wide angle x-ray scattering
CMC	Critical micelle concentrations
PV	Photovoltaic
TPP	Triphenyl phosphate
Chl-a	Chlorophyll A
STM	Scanning tunneling microscope
TCO	Transparent conductive oxide
ITO	Indium Tin oxide
FTO	Fluorine doped tin dioxide
LUMO	Lower unoccupied molecular orbital
TBAOH	Tetrabutylammonium hydroxide
Voc	Open circuit Voltage
Jsc	Short circuit current
IPCE	Incident Photon to Current Efficiency
FF	Fill factor
UV.VIS	Ultra violet visible

Vita

Rajab Emhemmed Abujnah was born on the Eighteen of November, 1964, in Al-khoms, Libya. He holds a BS.c in Environmental Studies from Sebha University College of Engineering and Technology Formally (Higher Institute of Technology) Brack Libya, since 1985, and MSc in Environmental Engineering from Saskatchewan University Saskatoon, Canada, since 1999. His Master's thesis was about evaluation of the effect of oily waste application on sandy soils on Oat growth and soil fertility. After his graduation he worked as research assistant in the department of Bio-agricultural Engineering at Saskatchewan University for two years and then joined the college of Science at Alemrgib University Alkhoms Libya where he work as a lecturer for 4 years. During this period of time he taught many courses (General Ecology, Environmental Technology, and Water Pollution). In addition to teaching he engaged in many environmental activities and was the main founder of the Division of Environmental Science in the college of Science at Al-Memrgib University. In reward of his hard work and achievement, he has awarded a PhD scholarship from the Ministry of Higher Education In Libya in 2006.

Rajab came to the United States in January, 2007 to join the Environmental Science and Engineering PhD program at the University of Texas at El Paso. During his stay at UTEP he published two papers; Abujnah, R. 2009 Environmental and Geological Consequences of the Libyan great Man Made River Project (GMMRP). Poster presented at: 2009 New Mexico Water Research Symposium, Macy Center, New Mexico Tech, Socorro, NM, August 11, 2009; Abujnah, R. 2008.The effects of oily waste on nutrients supply rate, as measured by cation and anion exchange membranes; The 7th International Symposium on Advanced Environmental Monitoring, 25-28 February 2008, Honolulu, Hawaii, USA. He also has pending USA patent titled as Asphaltene Based Photovoltaic Devices,

a United State Patent Application No 20090114283 U.S. Provisional Application Serial No. 61/224, 791132,

Permanent address: 213 Argonut Dr. # 40

El paso, TX, 79912

This dissertation was typed by Rajab Abujnah. Co-author Muhaned Abujnah